

# Flow Through a Throttle Body

A Comparative Study of Heat Transfer,  
Wall Surface Roughness and  
Discharge Coefficient

LIU-IEI-TEK-A-07/0071-SE

Per Carlsson, Linköping

February 23, 2007

## Copyright

The publishers will keep this document online on the Internet – or its possible replacement – for a period of 25 years starting from the date of publication barring exceptional circumstances. The online availability of the document implies permanent permission for anyone to read, to download, or to print out single copies for his/her own use and to use it unchanged for non-commercial research and educational purposes. Subsequent transfers of copyright cannot revoke this permission. All other uses of the document are conditional upon the consent of the copyright owner. The publisher has taken technical and administrative measures to assure authenticity, security and accessibility. According to intellectual property law, the author has the right to be mentioned when his/her work is accessed as described above and to be protected against infringement. For additional information about Linköping University Electronic Press and its procedures for publication and for assurance of document integrity, please refer to its www home page: <http://www.ep.liu.se/>.

© 2007 Per Carlsson.

## **Abstract**

When designing a new fuel management system for a spark ignition engine the amount of air that is fed to the cylinders is highly important. A tool that is being used to improve the performance and reduce emission levels is engine modeling where a fuel management system can be tested and designed in a computer environment thus saving valuable setup time in an engine test cell. One important part of the modeling is the throttle which regulates the air. The current isentropic model has been investigated in this report. A throttle body and intake manifold has been simulated using Computational Fluid Dynamics (CFD) and the influence of surface heating and surface wall roughness has been calculated. A method to calculate the effective flow area has been constructed and tested by simulating at two different throttle plate angles and several pressure ratios across the throttle plate. The results show that both surface wall roughness and wall heating will reduce the mass flow rate compared to a smooth and adiabatic wall respectively. The reduction is both dependent on pressure ratio and throttle plate angle. The effective area has showed to follow the same behaviour as the mass flow rate for the larger simulated throttle plate angle  $31^\circ$ , i.e. an increase as the pressure drop over the throttle plate becomes larger. At the smaller throttle plate angle  $21^\circ$ , the behaviour is completely different and a reduction of the effective area can be seen for the highest pressure drop where an increase is expected.



## Sammanfattning

När ett nytt bränslesystem ska designas till en bensinmotor är det viktigt att veta hur stor mängd luft som hamnar i cylindrarna. Ett verktyg som är på frammarsch för att förbättra prestanda och minska emissioner är modellbaserad simulering. Med hjälp av detta kan ett bränslesystem designas och testas i datormiljö och därigenom spara dyrbar tid som annars måste tillbringas i en motortestcell. En viktig del av denna modellering är spjället eller trotteln vilken reglerar luften. I denna rapport har studier gjorts på den nuvarande isentropiska modellen. Ett spjällhus och insugsrenör har simulerats med hjälp av Computational Fluid Dynamics (CFD) och påverkan av värme samt ytjämnhet på väggen har beräknats. En metod att beräkna den effektiva genomströmmade arean har konstruerats och testats vid två olika spjällvinklar samt flertalet tryckkvoter över spjället. Resultaten visar att både en uppvärmd vägg och en vägg med skrovlighet kommer att minska massflödet jämfört med en adiabatisk respektive en slät vägg. Minskningen har både spjällvinkel samt tryckkvots beroende. Den effektiva genomströmmade arean har visats sig följa samma beteende som massflödet vid den större simulerade spjällvinkeln  $31^\circ$ , det vill säga öka med ökat tryckfall över spjället. Vid den mindre vinkeln  $21^\circ$  är beteendet helt annorlunda jämfört med massflödet och en minskning av den effektiva arean kan ses vid det största tryckfallet där en ökning förväntades.



# Acknowledgments

I wish to express my gratitude to everyone who contributed to this work. I would especially like to thank Roland Gårdhagen, Division of Applied Thermodynamics and Fluid Mechanics, without his patience and encouragement this work had not been possible. His colleague Johan Renner that always took the time for a discussion. Professor Dan Loyd, Head of Division of Applied Thermodynamics and Fluid Mechanics. His constant source of knowledge and ability to understand my sometimes fuzzy ideas still surprise me. Associate Professor Lars Eriksson, Vehicular Systems Dept. of Electrical Engineering and Professor Matts Karlsson, Dept. of Biomedical Engineering that provided me with the problem. I would also like to thank Jonas Lantz and Joel Lundh for providing a good work climate and amusing discussions.

Linköping February 2007

Per Carlsson





# Contents

<b>1</b>	<b>Introduction</b>	<b>1</b>
1.1	Purpose . . . . .	2
<b>I</b>	<b>Throttle Flow</b>	<b>3</b>
<b>2</b>	<b>Background</b>	<b>5</b>
2.1	The complete Navier-Stokes Equations . . . . .	6
2.1.1	Equations of State . . . . .	7
2.2	Assumptions . . . . .	7
<b>3</b>	<b>Common Throttle Flow Estimation Models</b>	<b>11</b>
3.1	Flow Estimation Models . . . . .	11
3.1.1	Outflow Function $\Psi$ . . . . .	13
3.1.2	Throttle Area Equations . . . . .	13
3.1.3	Discharge Coefficient $C_d$ . . . . .	15
<b>II</b>	<b>Simulation and Analysis of Assumptions</b>	<b>17</b>
<b>4</b>	<b>Pre-simulation</b>	<b>19</b>
4.1	Geometry . . . . .	19
4.2	Mass or Pressure Driven Flow . . . . .	21
4.3	Solver . . . . .	22
4.4	Turbulence . . . . .	23
4.5	Criteria of Convergence . . . . .	24
4.6	Boundary and Internal Conditions . . . . .	25
4.7	Limitations . . . . .	26
<b>5</b>	<b>Analysis</b>	<b>29</b>
5.1	Ways of Comparison . . . . .	29
5.2	Estimating Effects of Wall Heating . . . . .	30
5.3	Estimating Effects of Wall Surface Roughness . . . . .	31
5.4	Calculating the Effective Flow Area . . . . .	32
5.5	Results . . . . .	35
5.6	Discussion . . . . .	38

5.6.1	Mesh Generation . . . . .	38
5.6.2	Wall Heat . . . . .	38
5.6.3	Wall Surface Roughness . . . . .	39
5.6.4	Effective Area . . . . .	39
5.7	Conclusions . . . . .	42
<b>6</b>	<b>Nomenclature</b>	<b>43</b>
<b>A</b>	<b>Results in Tabular Form</b>	<b>47</b>
<b>B</b>	<b>MATLAB Code</b>	<b>49</b>

# List of Figures

1.1	Throttle body with definition of angles, $\alpha_0 \neq 0$ to prevent wall binding	1
2.1	<b>(a)</b> Pressure ratio $\frac{p_2}{p_1}$ versus normalized mass flow rate, curves represent the isentropic model and Hendricks polytropic exponent model. <b>(b)</b> Isentropic model relative error compared with Hendricks polytropic exponent model. . . . .	5
3.1	Outflow function $\Psi$ , dotted line represents the isentropic model derived from the Navier-Stokes equations. Solid line is calculated by using Hendricks polytropic exponent model . . . . .	13
3.2	Area estimation comparison between simple geometrical model neglecting throttle shaft (dotted line) and more complex including throttle shaft (solid line) . . . . .	14
4.1	<b>(a)</b> Throttle body with pipe outlet. <b>(b)</b> Throttle plate and throttle shaft close-up. . . . .	19
4.2	<b>(a)</b> Throttle body with manifold exterior geometry. <b>(b)</b> : 1: Throttle plate, 2: Intake manifold, 3: Outlet, 4: Throttle shaft, 5: Inlet. . . . .	20
4.3	<b>(a)</b> Throttle body with decreased intake manifold volume to reduce number of computational cells whilst keeping the grid sufficiently dens. <b>(b)</b> Throttle plate and throttle shaft showing behind throttle body wall . . . . .	21
4.4	Flow chart describing the segregated solution method . . . . .	22
4.5	Flow chart describing the coupled solution method . . . . .	23
4.6	Internal energy with constant and polynomial $C_v$ . . . . .	26
5.1	<b>(a)</b> Example of a plane computational grid. <b>(b)</b> Complete exterior grid visual. . . . .	29
5.2	Example of grid used to downsample and calculate mean value and standard deviation. . . . .	30
5.3	Vena contracta forming after the minimum geometric cross sectional area. . . . .	32
5.4	<b>(a)</b> Pathlines releasing from throttle plate edge used to calculate the effective area. <b>(b)</b> Pathlines showing a contraction behind the throttle plate forming the effective area. . . . .	33
5.5	3D scatter plot of the points used to calculate the effective area. . . . .	34
5.6	<b>(a)</b> Scatter plot of points with maximum distance to center axis projected on the x-z plane enclosed with MATLAB function <i>convhull</i> . <b>(b)</b> Filled area with MATLAB function <i>polyarea</i> . . . . .	34

5.7	Mass flow rate and deviation from an adiabatic wall when investigating the influens of a heated wall. <i>Top</i> : Mass flow rate (observe the scale) at throttle plate angle, <i>left</i> : 31°, <i>right</i> : 21° . <i>Bottom</i> : Deviation from adiabatic wall. . . . .	35
5.8	Mass flow rate and deviation from a smooth wall when investigating the influens wall surface roughness roughness. <i>Top</i> : Mass flow rate (observe the scale) at throttle plate angle, <i>left</i> : 31°, <i>right</i> : 21° . <i>Bottom</i> : Deviation from smooth wall. . . . .	36
5.9	Coefficient of discharge calculated and measured with FLUENT, solid line represent $C_{d_{area}}$ and dotted $C_{d_{isentropic}}$ . <b>(a)</b> Throttle angle = 31°. <b>(b)</b> Throttle angle = 21° . . . . .	37
5.10	Static temperature field in K, $\Pi = 0.6$ , wall temperature 358 K. <b>(a)</b> : 21 degrees of throttle plate angle, <b>(b)</b> : 31 degrees of throttle plate angle. . . . .	39
5.11	Convergent - divergent nozzle forming downstream throttle edge . . . . .	41
5.12	Mach number exceeding one after the throttle plate . . . . .	41

# List of Tables

2.1	Throttle plate angle and corresponding cross sectional geometric area. .	6
4.1	Rounded mass flow rate with three significant figures . . . . .	24
4.2	Properties of the gas. . . . .	25
4.3	Inlet boundary conditions . . . . .	25
4.4	Outlet boundary conditions . . . . .	25
5.1	Heat transfered through walls and by the throttle - plate, edge and shaft	35
5.2	Integrated wall shear stress for each part when investigating the influence of wall surface roughness . . . . .	36
5.3	Number of cells and mass flow rate in geometry, mesh independence check.	38
A.1	Mass flow rate when investigating the influence of wall heating . . . . .	47
A.2	Mass flow rate when investigating the influence of wall surface roughness	47
A.3	Mass flow rate and coefficients of discharge. $C_{d_{area}}$ is calculated by measuring the effective area with the method presented in section 5.4, $C_{d_{area}} = \frac{A_{te}}{A_g}$ , $C_{d_{isentropic}} = \frac{\dot{m}_{simulated}}{\dot{m}_{isentropic}}$ . . . . .	48



# Chapter 1

## Introduction

To regulate the power output from an engine there have to be some restriction of how much fuel - air mixture that reaches the cylinders. One way to do this is to use some kind of valve that restricts the air, fuel is then regulated to get the correct fuel - air mixture. The most common valve is of butterfly type and is used in almost every car engine manufactured today, the valve is sketched in figure 1.1. The throttle plate rest angle  $\alpha_0$  is larger than zero to prevent wall binding.

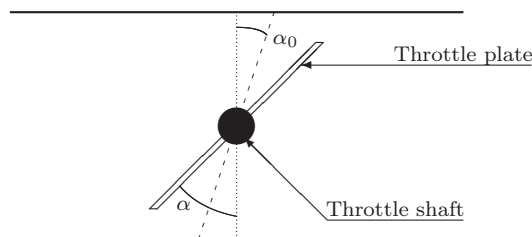


Figure 1.1: Throttle body with definition of angles,  $\alpha_0 \neq 0$  to prevent wall binding

Development of fuel injection systems that gives better fuel economy, less emissions and higher performance are central parts when a new engine is designed. This area is where most improvements have been made in the last two or three decades. In fuel management design simulation is one of the most powerful tools. This gives the engine control designer a way to run an artificial engine under controlled conditions controlling temperature, ambient pressure and other physical properties instantaneously without time loses. A real engine on the other hand may take several minutes and sometimes hours to reach steady state conditions. When simulating an engine the various engine components are divided into subsystems, for example, air filter, turbo charger, intercooler, throttle body, cylinders and exhaust system. For each subsystem there are equations or models that are used to describe how a particular subsystem will effect the others. If all subsystems are validated correctly against engine measurements they will behave and perform just as in the real engine. By doing so there are possibilities to get accurate results from simulations of how a real engine would react to a certain fuel management system.

## 1.1 Purpose

The main purpose of this report is to gain a greater understanding of how the air flow is restricted at the throttle plate and especially why the flow becomes choked at a certain pressure ratio using Computational Fluid Dynamics (CFD).



# Part I

## Throttle Flow



# Chapter 2

## Background

Engine measurements were conducted at The Department of Electrical Engineering, University of Linköping [1] only the results will be presented here. The engine data consists of measurements conducted at four different throttle plate angles presented with corresponding geometric cross sectional area in table 2.1.

The mass flow rate for the four throttle plate angles has been normalized and are presented in figure 2.1(a). The current model assuming isentropic flow, and Hendricks polytropic exponent model [7] are used to visualize differences. For further reading about the models see page 11 section 3.1.

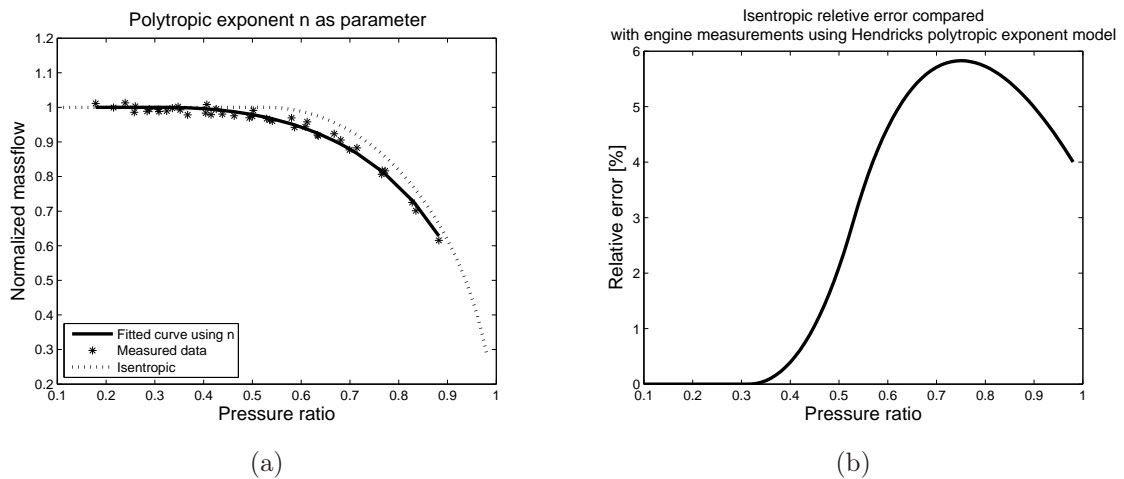


Figure 2.1: **(a)** Pressure ratio  $\frac{p_2}{p_1}$  versus normalized mass flow rate, curves represent the isentropic model and Hendricks polytropic exponent model. **(b)** Isentropic model relative error compared with Hendricks polytropic exponent model.

Throttle plate angle [°]	Area [mm <sup>2</sup> ]
19	150
17	125
15	100
13	75

Table 2.1: Throttle plate angle and corresponding cross sectional geometric area.

The model has a maximum relative error of approximately 6 percent, figure 2.1(b). However the “knee” where the flow is choked occurs at a different pressure ratio for the measured data compared with the isentropic model.

## 2.1 The complete Navier-Stokes Equations

The flow through the geometry is governed by three physical rules.

1. Conservation of mass.
2. Newtons second law,  $\mathbf{F} = m\mathbf{a}$ .
3. Conservation of energy.

These fundamental rules are used to derive the governing equations that are utilized to describe and calculate the flow. The equations are known as the complete Navier-Stokes equations, in conservation form and for a Newtonian fluid they are written as.

X direction.

$$\begin{aligned} \frac{\partial(\rho u)}{\partial t} + \frac{\partial(\rho u^2)}{\partial x} + \frac{\partial(\rho uv)}{\partial y} + \frac{\partial(\rho uw)}{\partial z} = -\frac{\partial p}{\partial x} + \frac{\partial}{\partial x} \left( \lambda \nabla \cdot \mathbf{V} + 2\mu \frac{\partial u}{\partial x} \right) \\ + \frac{\partial}{\partial y} \left[ \mu \left( \frac{\partial v}{\partial x} + \frac{\partial u}{\partial y} \right) \right] + \frac{\partial}{\partial z} \left[ \mu \left( \frac{\partial u}{\partial z} + \frac{\partial w}{\partial x} \right) \right] + \rho f_x \end{aligned} \quad (2.1)$$

Y direction.

$$\begin{aligned} \frac{\partial(\rho v)}{\partial t} + \frac{\partial(\rho uv)}{\partial x} + \frac{\partial(\rho v^2)}{\partial y} + \frac{\partial(\rho vw)}{\partial z} = -\frac{\partial p}{\partial y} + \frac{\partial}{\partial x} \left[ \mu \left( \frac{\partial v}{\partial x} + \frac{\partial u}{\partial y} \right) \right] \\ + \frac{\partial}{\partial y} \left( \lambda \nabla \cdot \mathbf{V} + 2\mu \frac{\partial v}{\partial y} \right) + \frac{\partial}{\partial z} \left[ \mu \left( \frac{\partial w}{\partial y} + \frac{\partial v}{\partial z} \right) \right] + \rho f_y \end{aligned} \quad (2.2)$$

Z direction.

$$\begin{aligned} \frac{\partial(\rho w)}{\partial t} + \frac{\partial(\rho uw)}{\partial x} + \frac{\partial(\rho vw)}{\partial y} + \frac{\partial(\rho w^2)}{\partial z} = -\frac{\partial p}{\partial z} + \frac{\partial}{\partial x} \left[ \mu \left( \frac{\partial u}{\partial z} + \frac{\partial w}{\partial x} \right) \right] \\ + \frac{\partial}{\partial y} \left[ \mu \left( \frac{\partial w}{\partial y} + \frac{\partial v}{\partial z} \right) \right] + \frac{\partial}{\partial z} \left( \lambda \nabla \cdot \mathbf{V} + 2\mu \frac{\partial w}{\partial z} \right) + \rho f_z \end{aligned} \quad (2.3)$$

Energy equation.

$$\begin{aligned}
 \frac{\partial}{\partial t} \left[ \rho \left( e + \frac{V^2}{2} \right) \right] + \nabla \cdot \left[ \rho \left( e + \frac{V^2}{2} \right) \mathbf{V} \right] &= \rho \dot{q} \\
 + \frac{\partial}{\partial x} \left( k \frac{\partial T}{\partial x} \right) + \frac{\partial}{\partial y} \left( k \frac{\partial T}{\partial y} \right) + \frac{\partial}{\partial z} \left( k \frac{\partial T}{\partial z} \right) - \frac{\partial(up)}{\partial x} - \frac{\partial(vp)}{\partial y} - \frac{\partial(wp)}{\partial z} \\
 + \frac{\partial(u\tau_{xx})}{\partial x} + \frac{\partial(u\tau_{yx})}{\partial y} + \frac{\partial(u\tau_{zx})}{\partial z} + \frac{\partial(v\tau_{xy})}{\partial x} + \frac{\partial(v\tau_{yy})}{\partial y} + \frac{\partial(v\tau_{zy})}{\partial z} \\
 + \frac{\partial(w\tau_{xz})}{\partial x} + \frac{\partial(w\tau_{yz})}{\partial y} + \frac{\partial(w\tau_{zz})}{\partial z} + \rho \mathbf{f} \cdot \mathbf{V} \quad (2.4)
 \end{aligned}$$

### 2.1.1 Equations of State

The air traveling past the throttle plate is assumed to be an ideal gas, i.e. the ideal gas law can be utilized

$$p = \rho RT \quad (2.5)$$

For a calorically perfect gas the relation between temperature and internal energy is

$$e = c_v T \quad (2.6)$$

## 2.2 Assumptions

One way to solve the complete Navier-Stokes equations analytically is to reduce them with assumptions. However with every assumption made the expression loses in accuracy. To derive the equations that are the foundation to most models that are used to describe the flow the following suppositions are made.

- The flow is assumed one directional, lets say in the X direction.  $v = w = \frac{\partial}{\partial y} = \frac{\partial}{\partial z} = 0$ .
- The gas is assumed ideal,  $p = \rho RT$ .
- The flow is assumed to be at steady state,  $\frac{\partial}{\partial t} = 0$ .
- The gas is assumed to have a constant specific heat,  $e = c_v T$ .
- Body forces are neglected,  $f_x = f_y = f_z = 0$ .
- Viscosity is neglected in the system,  $\mu = \lambda = 0$ .
- Thermal conductivity is neglected,  $k = 0$ .
- No heat is added through the wall,  $\dot{q} = 0$ .

Equations 2.1 - 2.4 can now be reduced to Continuity equation.

$$\frac{\partial(\rho u)}{\partial x} = 0 \quad (2.7)$$

Momentum equation.

$$\frac{\partial(\rho u^2)}{\partial x} = -\frac{\partial p}{\partial x} \quad (2.8)$$

Energy equation.

$$\frac{\partial}{\partial x} \left[ \rho \left( e + \frac{u^2}{2} \right) u \right] = -\frac{\partial(up)}{\partial x} \quad (2.9)$$

From equation 2.5 we get the derivative of  $p$ .

$$\frac{\partial p}{\partial x} = R \left( \rho \frac{\partial T}{\partial x} + T \frac{\partial \rho}{\partial x} \right) \quad (2.10)$$

By including the cross sectional area  $A$  to equation 2.7 we get the expression for the continuity equation

$$\frac{\partial(\rho u A)}{\partial x} = \rho A \frac{\partial u}{\partial x} + \rho u \frac{\partial A}{\partial x} + u A \frac{\partial \rho}{\partial x} = 0 \quad (2.11)$$

or

$$\rho_1 u_1 A_1 = \rho_2 u_2 A_2 \quad (2.12)$$

This is valid at every point 1 and 2 in the flow. For simplicity index 1 means at inlet and 2 at the throat. The equations for momentum and energy can be derived in a similar way, see any good book about fluid dynamics e.g. [5]

Momentum equation.

$$p_1 A_1 + \rho_1 V_1^2 A_1 + \int_{A_1}^{A_2} p \, dA = p_2 A_2 + \rho_2 V_2^2 A_2 \quad (2.13)$$

Energy equation.

$$h_1 + \frac{u_1^2}{2} = h_2 + \frac{u_2^2}{2} \quad (2.14)$$

By assuming a isentropic process the relations between pressure, density and temperature can be summarized as

$$\left( \frac{p_2}{p_1} \right) = \left( \frac{\rho_2}{\rho_1} \right)^\gamma = \left( \frac{T_2}{T_1} \right)^{\frac{\gamma}{\gamma-1}} \quad (2.15)$$

Furthermore the total temperature can be written in terms of static temperature as

$$T^o = T + \frac{u^2}{2c_p} \quad (2.16)$$

an other important property is the speed of sound which is described by

$$a = \sqrt{\gamma RT} = \sqrt{\frac{2\gamma}{\gamma+1} RT^o} \quad (2.17)$$

When the velocity at the throat is at Mach one the mass flow will not increase. This is called choked flow. The flow is driven by the pressure ratio which can be described using inlet temperatures.

$$\frac{p_2}{p_1} = \left( \frac{T_1^o}{T_1} \frac{2}{\gamma + 1} \right)^{\frac{\gamma}{\gamma-1}} \quad (2.18)$$

From these equations an expression for the nozzle flow can be derived. The pressure at the throat.

$$p_2^* = \max \left\{ p_2, p_1 \left( \frac{T_1^o}{T_1} \frac{2}{\gamma + 1} \right)^{\frac{\gamma}{\gamma-1}} \right\} \quad (2.19)$$

The velocity at the throat.

$$u_2 = \sqrt{u_1^2 + 2c_p T_1 \left( 1 - \left( \frac{p_2^*}{p_1} \right)^{\frac{\gamma}{\gamma-1}} \right)} \quad (2.20)$$

The density at the throat.

$$\rho_2 = \frac{p_2^*}{RT_2} \quad (2.21)$$

If the inlet velocity  $u_1 \ll u_2$  we finally get the expression for one dimensional isentropic ideal flow.

$$\left\{ \begin{array}{l} \Pi = \max \left\{ \frac{p_2}{p_1}, \left( \frac{2}{\gamma+1} \right)^{\frac{\gamma}{\gamma-1}} \right\} \\ \Psi(\Pi) = \sqrt{\frac{2\gamma}{\gamma-1} \left( \Pi^{\frac{2}{\gamma}} - \Pi^{\frac{\gamma+1}{\gamma}} \right)} \\ \dot{m} = \frac{p_1}{\sqrt{RT_1}} A \Psi(\Pi) \end{array} \right. \quad (2.22)$$





# Chapter 3

## Common Throttle Flow Estimation Models

From the engine measurements presented in section 2 one can see that the isentropic model is a quite good approximation of the mass flow rate, but since the throttle model only is a subsystem which will effect other subsystem in the engine simulation the error can escalate leading to greater divergence in the final result. It is therefore vital to adjust the model so it fits perfect to engine measurement. This can be done in mainly two ways.

- Adjusting the mass flow rate as a lumped system.
- Adjusting parameters separately i.e. effective area, velocity at throat, density.

If one is only interested in the mass flow rate they both give accurate results with proper validation. By lumping the differences in one single term interesting fluid mechanics phenomenons may be lost.

### 3.1 Flow Estimation Models

Standard expression [8] equation 2.22 derived in section 2.2. By adding the coefficient of discharge  $C_d$  adjustments can be made so that the expression fits to measured data.

$$\dot{m}(\alpha, p_{after}, p_{before}, T_{before}) = \frac{p_{before}}{\sqrt{R_a T_{before}}} \Psi(\Pi) C_d A(\alpha) \quad (3.1)$$

$$\Psi(\Pi) = \begin{cases} \sqrt{\frac{2\gamma}{\gamma-1} \left( \Pi^{\frac{2}{\gamma}} - \Pi^{\frac{\gamma+1}{\gamma}} \right)} & \text{for } \Pi > \left( \frac{2}{\gamma+1} \right)^{\frac{\gamma}{\gamma-1}} \\ \sqrt{\frac{2\gamma}{\gamma-1} \left( \left( \frac{2}{\gamma+1} \right)^{\frac{2}{\gamma-1}} - \left( \frac{2}{\gamma+1} \right)^{\frac{\gamma+1}{\gamma-1}} \right)} & \text{otherwise} \end{cases} \quad (3.2)$$

The expression can be modified [7] with use of tunable parameters.

$$\dot{m}(\alpha, p_a, p_i, T_a) = \dot{m}_{at1} \frac{p_a}{\sqrt{T_a}} \beta_1(\alpha) \beta_2(p_r) \quad (3.3)$$

$$\beta_1(\alpha) = 1 - \alpha_1 \cos(\alpha) + \alpha_2 \cos^2(\alpha) \quad (3.4)$$

$$\beta_2(p_r) = \begin{cases} \frac{1}{p_n} \sqrt{p_r^{p'_1} - p_r^{p'_2}} & \text{if } p_r \geq p_c \\ 1 & \text{if } p_r < p_c \end{cases} \quad (3.5)$$

$$p_c = \Pi_{crit} = \left[ \frac{p'_1}{p'_2} \right]^{\left( \frac{1}{p'_2 - p'_1} \right)} \quad (3.6)$$

$$p_n = \sqrt{p_c^{p'_1} - p_c^{p'_2}} \quad (3.7)$$

$$p_r = \Pi = \frac{p_i}{p_a} \quad (3.8)$$

Equation 3.1 comes as a direct derivation from the Navier-Stokes equations assuming isentropic flow and only the discharge coefficient is added as a fitting parameter. Equation 3.1 consists of three independent fitting parameters  $\dot{m}_{at1}$ ,  $\beta_1$  and  $\beta_2$ .  $\beta_1$  serves as an area dependent discharge coefficient,  $\beta_2$  has similarities with the outflow function  $\Psi$  and  $\dot{m}_{at1}$  is used as a fitting constant.

### 3.1.1 Outflow Function $\Psi$

The outflow function  $\Psi$  is derived from the velocity and the density at the throat. The function determines at which pressure ratio the flow becomes choked, see figure 3.1. Observe that Hendricks in equation 3.5 refers to  $\Psi$  as  $\beta_2$ .

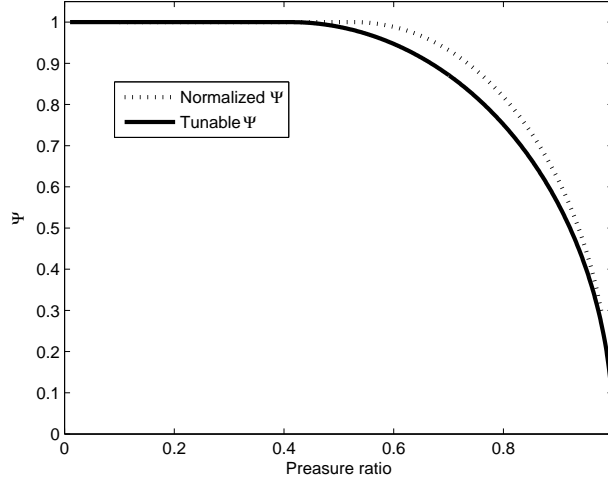


Figure 3.1: Outflow function  $\Psi$ , dotted line represents the isentropic model derived from the Navier-Stokes equations. Solid line is calculated by using Hendricks polytropic exponent model

For the standard expression equation 3.2 the pressure ratio when the flow is choked can be calculated by.

$$\Pi_{crit} = \left( \frac{2}{n+1} \right)^{\frac{n}{n-1}} = 0.5283 \text{ at } n = \gamma = 1.4 \quad (3.9)$$

With parameters  $p'_1$  and  $p'_2$ , the polytropic exponent  $n$  is adjusted to determine the critical pressure ratio when using Hendricks model.  $\Pi_{crit} = 0.4125$  fits well to the measured engine data. Solving equation 3.9 with respect to  $n$  will result in  $n = 2.3$  for the given critical pressure ratio.

### 3.1.2 Throttle Area Equations

The geometrical cross sectional area which the flow has to pass can be calculated by using models of various complexity. The simplest one which neglects the throttle shaft is described by.

$$A_g(\alpha) = \frac{\pi D^2}{4} \left( 1 - \frac{\cos(\alpha)}{\cos(\alpha_0)} \right) \quad (3.10)$$

By including the throttle shaft diameter  $b$ , a more accurate expression is acquired [8].

$$A_g(\alpha) = \frac{\pi D^2}{4} \left[ \left( 1 - \frac{\cos(\alpha)}{\cos(\alpha_0)} \right) + \frac{2}{\pi} \left[ \frac{b}{\cos(\alpha)} (\cos^2(\alpha) - b^2 \cos^2 \alpha_0)^{1/2} + \frac{\cos(\alpha)}{\cos(\alpha_0)} \sin^{-1} \left( \frac{b \cos(\alpha_0)}{\cos(\alpha)} \right) - b(1 - b^2)^{1/2} - \sin^{-1}(b) \right] \right] \quad (3.11)$$

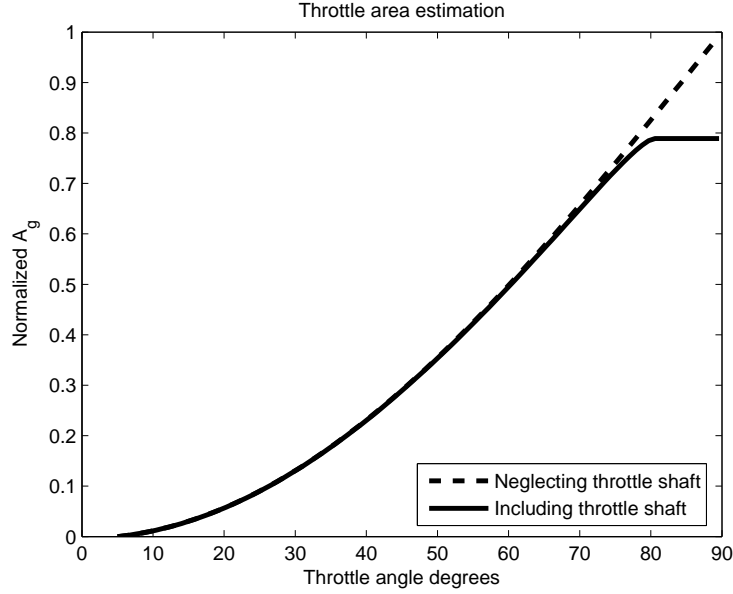


Figure 3.2: Area estimation comparison between simple geometrical model neglecting throttle shaft (dotted line) and more complex including throttle shaft (solid line)

The area estimation model can be a great source of error. Neither the model with or without throttle shaft include throttle plate thickness. In two dimensions it can be showed that a systematic error proportional to the throttle plate thickness occurs [10].

$$\alpha_{actual} = \alpha - \arctan \left( \frac{1}{\left(\frac{D}{t}\right) \cos(\alpha_0) - \tan(\alpha_0)} \right) \quad t = \text{Throttle plate thickness} \quad (3.12)$$

### Leak Area

At small throttle angles the leak area at the throttle plate plays a dominant role. One should keep in mind that this occurs at pressure ratio that are relatively small to very small compared to larger throttle angles. It is therefore crucial to included the throttle leak area in the equation used to estimate throttle area, i.e.

$$A_g(\alpha) = A_g(\alpha) + A_{Leak} \quad (3.13)$$

Pursifull [12] concludes from engine experiments that leak area is about 15 percent of total area at a throttle angle of 4 degrees for his particular throttle body. At larger angles the relative error caused by neglecting leak area obviously gets smaller. The leak area must be determined for each individual throttle body.

### 3.1.3 Discharge Coefficient $C_d$

The discharge coefficient ranging from 0 to 1 is a coefficient that describes how much the actual flow differs from a reference flow through the same restriction and geometry. There is no distinct definition of  $C_d$  but several authors have given there own interpretation.

#### The isentropic discharge coefficient

By measuring the mass flow rate and dividing it with the isentropic mass flow rate one get the expression for the isentropic discharge coefficient [3].

$$C_{d_{is}} = \frac{\text{measured mass flow rate}}{\text{isentropic nozzle mass flow rate}} = \frac{\dot{m}_{ex}}{\dot{m}_{is}} \quad (3.14)$$

By analysis of the First Law of Thermodynamics and the continuity equation one can derive equation 3.15, assuming that deviations in the model are solely dependent on the effective cross sectional area.

$$A_{te} = \frac{\dot{m}_{ex} \sqrt{\gamma R T_1}}{\gamma p_1 \left(\frac{p_2}{p_1}\right)^{\frac{1}{\gamma}} \sqrt{\frac{2}{\gamma-1} \left(1 - \left(\frac{p_2}{p_1}\right)^{\frac{\gamma-1}{\gamma}}\right)}} \quad (3.15)$$

$$\dot{m}_{is} = \rho_t A_{te} u_t = \rho_2 A_2 u_2 \quad (3.16)$$

Equation 3.14 can thus be written as.

$$C_{d_{is}} = \frac{\text{effective throat area}}{\text{geometrical throat area}} = \frac{A_{te}}{A_g} = \frac{A_{te}}{A_2} \quad (3.17)$$

#### Ideal discharge coefficient

Flow coefficient [8] or ideal discharge coefficient [3].

$$C_d = \frac{\text{actual mass flow rate}}{\text{ideal mass flow rate}} = \frac{\dot{m}_{ex}}{\dot{m}_{id}} \quad (3.18)$$

An other way to treat the discharge coefficient is to define it in terms of an effective cross sectional area of the passage and a reference area [8].

$$C_d = \frac{A_E}{A_R} \quad (3.19)$$

Here the reference area  $A_R$  is usually taken as the minimum cross-sectional area. The effective area  $A_E$  is a bit more arbitrary. One definition is that the effective area is the cross sectional area which ideal frictionless flow would pass at a restriction between a large upstream reservoir and a large downstream reservoir.

### Actual discharge coefficient

$$C_{da} = \frac{\text{effective throat area}}{\text{geometrical throat area}} = \frac{A_{te}}{A_g} = \frac{A_{te}}{A_2} \quad (3.20)$$

The similarity with equations 3.17 and 3.19 are obvious [3].

### $C_d$ as function of $\Pi$ and $A(\alpha)$

It stands clear from the previous equations 3.14 - 3.20 that the discharge coefficient has a dependency on both the pressure ratio  $\Pi$  and the area  $A(\alpha)$ . Blair [3] uses maps to determine the  $C_d$  for specific area and pressure ratio  $\Pi$ , this suggests that

$$C_d = C_d(\Pi, A(\alpha)) \quad (3.21)$$

Andersson [1] on the other hand concludes from engine experiments that equation 3.21 can be separated in two products i.e.

$$C_d = C_d(\Pi, A(\alpha)) = C_d(\Pi)C_d(A(\alpha)) \quad (3.22)$$

On a naturally aspirated engine  $C_d$  can be treated as a function of throttle angle  $\alpha$  only. By experiments conducted by Pursifull [12]  $C_d$  ranges from 0.7 to 1.05, the value 1.05 is nonphysical but fits well to his measured data.

### Which model of $C_d$ is correct

It is apparent that there is no distinct definition of  $C_d$ . An other problem which adds to this is that  $C_d$  also is dependent on geometry of the actual throttle body. By this meaning that the edge of the throttle plate, the throttle body wall finish and other properties will influence  $C_d$  and this is individual to each and every throttle body. There is also the problem with adapting a two dimensional area to a three dimensional flow [12].  $C_d$  will be discussed more in section 5.4 on page 32

## Part II

# Simulation and Analysis of Assumptions





# Chapter 4

## Pre-simulation

### 4.1 Geometry

Initial simulations were conducted on a pipe 300 *mm* long with a diameter of 60 *mm*, the throttle plate rest angle  $\alpha_0$  where  $5^\circ$ . The throttle shaft center axis where located 100 *mm* from the inlet. This setup was soon rejected since the outlet had a to big influence of the flow at the throttle plate and was not seen as a proper representation of the actual flow. In order to overcome the problem with outlet boundary influence the pipe was lengthened 800 *mm*. Both the geometry and the mesh were created using the commercially available computer software ANSYS ICEM CFD (2005, ANSYS Inc).

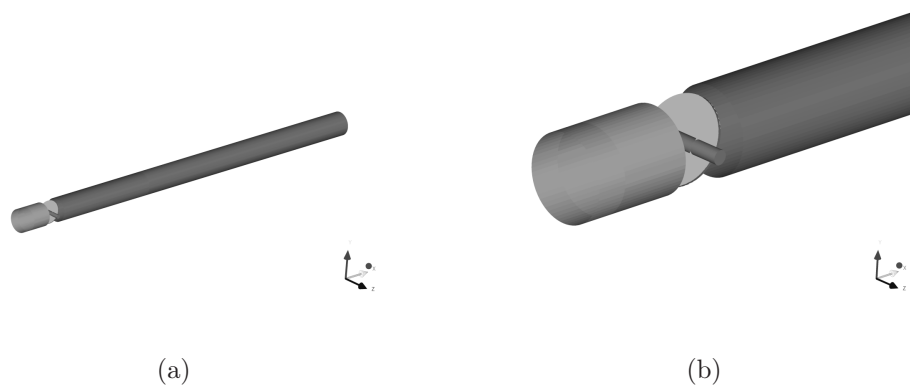


Figure 4.1: **(a)** Throttle body with pipe outlet. **(b)** Throttle plate and throttle shaft close-up.

The fluid volume of the geometry in figure 4.1 is 3087  $cm^3$ . There is a problem with having a large volume while creating the computational mesh, large total volume means that number of cells have to be substantial. The gap between the throttle plate and the throttle body wall is very small, a consequence of this is that cells also need to be small. One way to overcome this is to use different sizes of cells, small cells near and at the gap and larger in general. The transition between these different cell densities

can cause problems with warped cells and poor mesh quality as a result. In an attempt to decrease the total volume a more realistic geometry were designed with an intake manifold and four outlets. The flow is now interrupted by the lower manifold wall and the setup were considered more alike the real geometry.

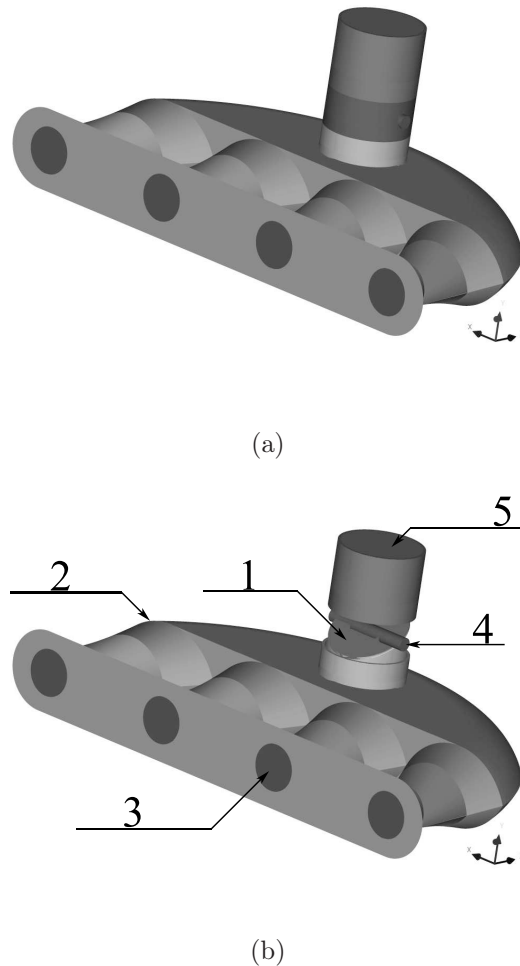


Figure 4.2: (a) Throttle body with manifold exterior geometry. (b): 1: Throttle plate, 2: Intake manifold, 3: Outlet, 4: Throttle shaft, 5: Inlet.

For the geometry in figure 4.2 the fluid volume is  $2734 \text{ cm}^3$ . Simulation gave evenly distributed mass flow to each outlet but there were still problems with mesh density. The mesh was considered too coarse to resolve boundary layers. In an attempt to decrease the volume furthermore adjustments were made to the intake manifold. This adjustment was not wanted since a geometry with good flow properties and evenly distributed flow already existed. But the change was necessary due to computer limitations while generating the mesh.

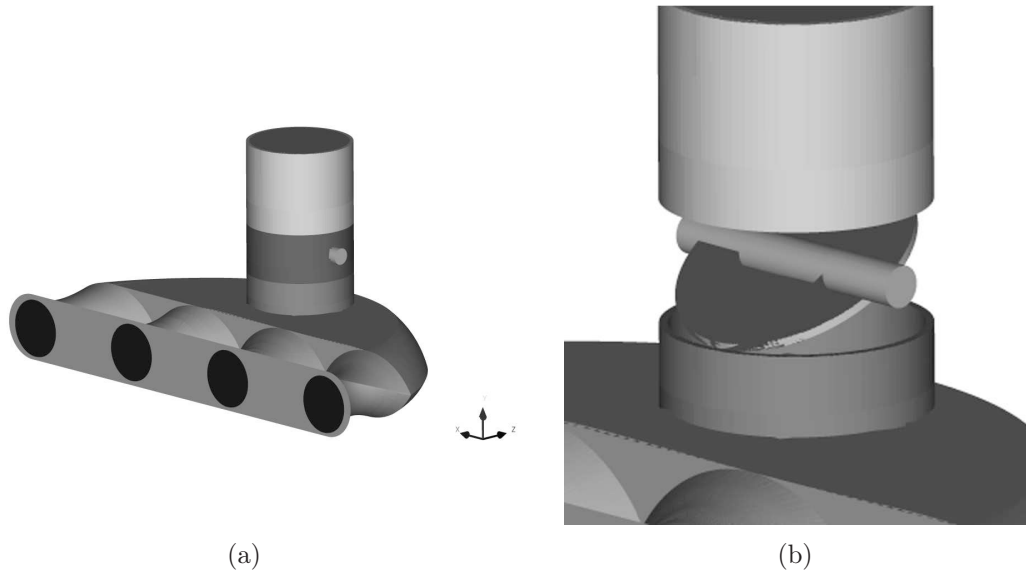


Figure 4.3: **(a)** Throttle body with decreased intake manifold volume to reduce number of computational cells whilst keeping the grid sufficiently dens. **(b)** Throttle plate and throttle shaft showing behind throttle body wall

From the final geometry, figure 4.3 with fluid volume of  $1182 \text{ cm}^3$  only the throttle plate angle where changed. The throttle shaft is located  $65 \text{ mm}$  from the inlet, the throttle body diameter is  $60 \text{ mm}$  and the throttle plate rest angle is  $5^\circ$ . Two meshes with different throttle plate angle,  $21^\circ$  and  $31^\circ$  where design both with unstructured tetrahedral cells. For  $21^\circ$  the total number of computational cells were 2.3 million and for  $31^\circ$ , 2.7 million.

## 4.2 Mass or Pressure Driven Flow

In FLUENT 6.1 (1998, Fluent Inc) there are two ways to drive the flow through the geometry when using compressible models for this particular problem.

- Static mass flow rate at inlet and static pressure outlets, mass driven flow.
- Static pressure inlet and static pressure outlets, pressure driven flow.

Initial simulations were conducted using mass driven flow. The boundary conditions are very easy to set and the solution converges fast. There is one great disadvantage by using mass driven flow though, as the pressure ratio gets close to the critical one continuity is compromised. The flow is choked at the throttle plate and therefore the mass flow rate at the outlets is stabilized but the pressure before the throttle will increase as additional mass is introduced in the cavity. This will lead to divergence as the pressure peaks in front of the throttle plate. For this reason one must be careful not to use mass driven flow close to or under the critical pressure ratio.

Pressure driven flow has no limited operating range seen so far. The pressure driven flow is much more sensitive to initial conditions than the mass driven one. As for the

mass driven flow initial conditions are computed from the inlet. In the mass flow driven case there is no problem setting a initial velocity to zero at the inlet. In the simulations conducted with pressure driven flow initial velocities at the inlet has been set a bit arbitrary. Velocities around 30-50 m/s at the inlet has showed to give good results. The main problem is if the initial velocity is set to high this will lead to a divergent solution caused by pressure build up in front of the throttle plate or sudden decrease in temperature near the throat caused by super sonic flow conditions.

### 4.3 Solver

There are two numerical methods available in FLUENT to solve the governing equations (mass, momentum and energy) and in this case also turbulence.

- segregated solver
- coupled solver

With the segregated solver FLUENT will solve the equations sequentially by this meaning one at a time. Since the governing equations are coupled and non-linear several iterations must be performed to reach a converged solution. The process is described in figure 4.4.

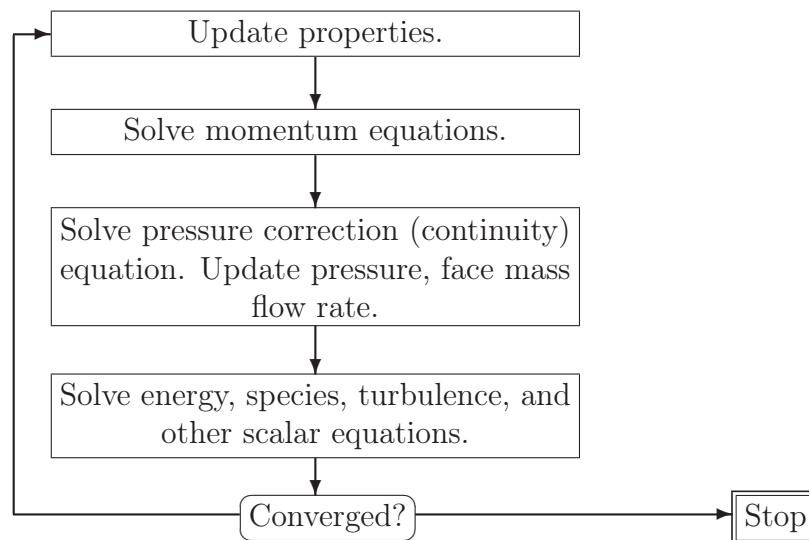


Figure 4.4: Flow chart describing the segregated solution method

The coupled solver solves the governing equations (mass, momentum and energy) coupled together. As for the segregated solver method several iterations must be performed to reach a converged solution. The coupled solution method is illustrated in figure 4.5.

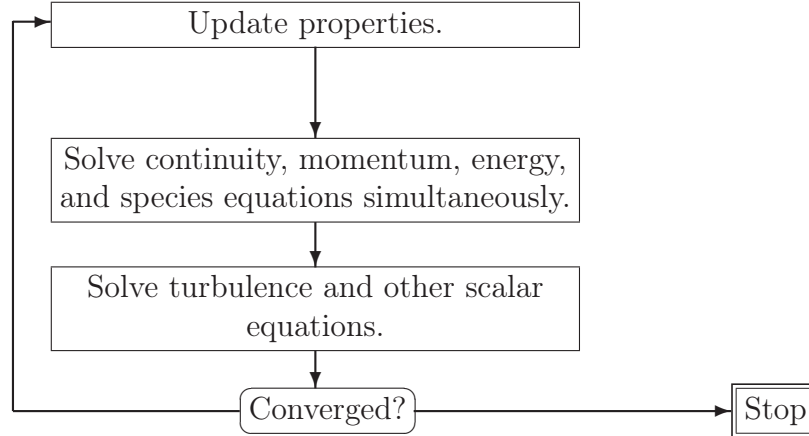


Figure 4.5: Flow chart describing the coupled solution method

Throughout the simulation it is necessary to control the change of the flow field. FLUENT uses an under-relaxation procedure which reduces the change of a specific variable after each iteration. This can be described using a scalar quantity  $\Phi$ .

$$\Phi = \Phi_{old} + \delta\Delta\Phi \quad (4.1)$$

By decreasing  $\delta$  the convergence gets more controlled and the author has reduced this from the default value 0.3 to 0.1 for the pressure update step in order to get a converged solution. Early attempts were made with the default value, resulting in divergence after just a few iterations. Only the segregated solver uses the under-relaxation feature. It should be noticed that decreasing the under relaxation value will cause slower convergence. All simulations were conducted with the segregated solver.

## 4.4 Turbulence

To find a universal turbulence model that describes the flow at all circumstances is just not possible, atleast not for now. The turbulence models available in FLUENT have all their own limitations. The overall criteria for the simulations has been to get a fast converging solution. The k -  $\epsilon$  model with standard wall function was used since it gave good performance of the overall calculations. The boundary conditions for turbulence kinetic energy at both inlet and the outlets can be calculated by [6],

$$k = \frac{3}{2} (u_{avg}I)^2 \quad (4.2)$$

where  $I$  is the turbulence intensity,

$$I = 0.16 (Re_{DH})^{-\frac{1}{8}} \quad (4.3)$$

The dissipation rate can be calculated by

$$\epsilon = C_{\mu}^{(3/4)} \frac{k^{3/2}}{\ell} \quad (4.4)$$

where

$$\ell = 0.007D \quad (4.5)$$

The author's intent was to study different turbulence models and boundary conditions but due to time and computer limitations this could not be realized. Furthermore it has been showed [9] that the standard k -  $\epsilon$  turbulent model gives the best prediction of discharge coefficient and critical pressure ratio of gas flow through a critical Laval nozzle compared with other turbulent models. This however will not eliminate anomalies that can be derived from the turbulence model.

## 4.5 Criteria of Convergence

There are no stand alone model or measurement to determine if a solution is fully converged. In FLUENT one can monitor the following residuals for the specific problem.

- Continuity
- X-velocity
- Y-velocity
- Z-velocity
- Energy
- Turbulence k
- Turbulence  $\epsilon$

In addition to this the mass imbalance have been calculated between inlet and outlets. This net mass flow in combination with the residuals are used to determine if the solution is converged. The absolute net mass imbalance value ( $|\dot{m}_{net}|$ ) is not allowed to be greater than  $5 \cdot 10^{-5} \frac{kg}{s}$ . The residual plots themselves were used to check if the solution had leveled off or had a steady decrease in a substantial amount of iterations. However additional iterations where ran to ensure convergence. The criteria  $|\dot{m}_{net}| < 5 \cdot 10^{-5} \frac{kg}{s}$  is used as a maximum value but for most of the simulations this term was in order of  $5 \cdot 10^{-6} \frac{kg}{s}$  or less. The choice of  $|\dot{m}_{net}|$  has been made in such a way that the overall mass flow rate will have at least three significant figures. An example is given in table 4.1

Variable	Mass flow rate $\frac{kg}{s}$
$\dot{m}$	0.072162233
$\dot{m}_{net}$	$1.63e - 6$
$\dot{m}_{rounded}$	0.0722

Table 4.1: Rounded mass flow rate with three significant figures

## 4.6 Boundary and Internal Conditions

The gas has been treated as air with ideal gas properties. For further reading about this see section 4.7 on page 26.

All walls including the throttle plate and shaft were treated as adiabatic and perfectly smooth in all cases except when surface wall roughness and wall heating were simulated. At the inlet atmospheric pressure at sea level where set as a boundary conditions.

The pressure at the outlets has been set in correlation with the inlet pressure thus achieving an appropriate pressure ratio.

$$p_{outlets} = \Pi \cdot p_{inlet} \quad (4.6)$$

Equal pressure at all outlets is obviously not what happens in an real engine. The method is used to assure that a homogeneous pressure field with small pressure gradients is produced in the intake manifold since the throttle body is of main interest. Details of boundary conditions for inlet, outlets and the gas it self are summerized in tables 4.2 to 4.4.

Gas Property	Value	Unit
$C_p$	1006.43	$\frac{J}{kgK}$
Thermal Conductivity	0.0242	$\frac{W}{mK}$
Viscosity	$1.7894e - 5$	$\frac{kg}{ms}$
Molecular Weight	28.966	$\frac{1}{mol}$

Table 4.2: Properties of the gas.

Inlet Boundary	Value	Unit
Total Temperature	300	$K$
Turbulence Kinetic Energy	0.5	$\frac{m^2}{s^2}$
Turbulence Dissipation Rate	2	$\frac{m^2}{s^3}$
Gauge Total Pressure	101300	$Pa$

Table 4.3: Inlet boundary conditions

Outlet Boundary	Value	Unit
Backflow Total Temperature	300	$K$
Backflow Turbulence Kinetic Energy	0.5	$\frac{m^2}{s^2}$
Backflow Turbulence Dissipation Rate	2	$\frac{m^2}{s^3}$
Gauge Pressure	$\Pi \cdot 101300$	$Pa$

Table 4.4: Outlet boundary conditions

The backflow conditions are only in use if any backflow occurs, otherwise only the pressure will act as an boundary condition.

## 4.7 Limitations

The specific heat has been treated as constant. There are possibilities to simulate polynomial, piecewise linear or piecewise polynomial specific heat. In figure 4.6 a comparison between constant  $C_v$  and polynomial  $C_v$  can be seen. The polynomial is written as.

$$C_v = a + bT + cT^2 + dT^3, \quad a, b, c, d \text{ constants} \quad (4.7)$$

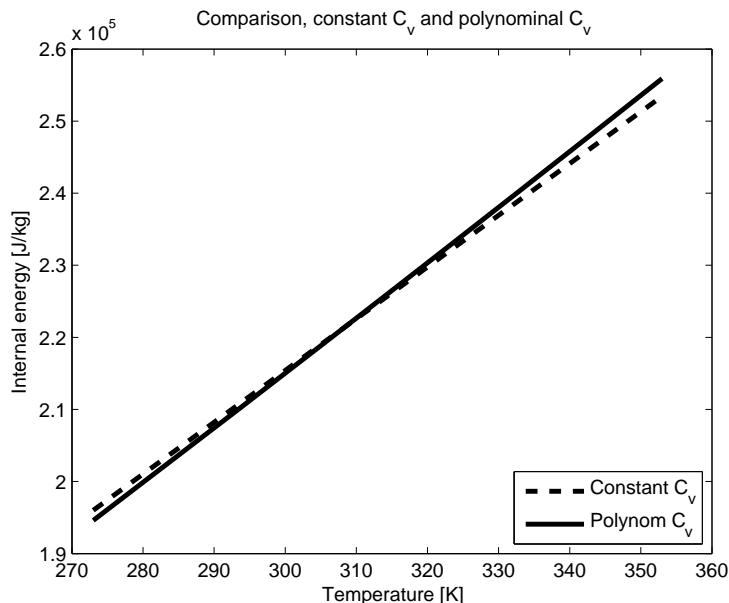


Figure 4.6: Internal energy with constant and polynomial  $C_v$

The polynomial expression has a maximum error of 0.72 percent [4] in the temperature range  $273 - 1800 K$ . If we use the model with constant  $C_v$  and compare it with the polynomial  $C_v$  the maximum deviation is approximately one percent. The maximum total error of the constant expression will therefore not be more than roughly 2 percent if the two maximum errors coincide.

Throughout the simulations the air has been treated as an ideal gas. A gas can be treated as ideal if the pressure is low and the temperature is sufficiently high. For air that consists of mainly nitrogen the critical temperature point is at  $132.5 K$  and critical pressure point is at  $3.77 MPa$ . The lowest temperatures observed in the simulations has been in the order of  $150 K$  for  $\Pi = 0.2$ . If this is regarded as sufficiently high the gas can be treated as ideal with an error less than one percent [4].

The mass forces has been seen as highly negligible, a result of the high velocities in the geometry. The only known mass force acting on the flow is gravity. This have an effect in sedimentation process where velocities are dominated by mass forces but in this particular case they are neglected.



There are physical properties that have a temperature dependency, this includes viscosity and thermal conductivity that has been held constant throughout the simulations. To see what effect the thermal conductivity had on the result two test simulations were made with two different values for the thermal conductivity.

To reduce speed at the throat pressure ratio  $\Pi$  were kept at a moderate 0.9. The assumption is that the thermal conductivity will have greater effect at smaller velocities since the heat will have more time to spread. Even at this high pressure ratio the average velocity at the throat is in the area of  $100 \frac{m}{s}$ . To get a substantial difference between the two simulations the thermal conductivity  $k$  were held constant at  $0.024 \frac{W}{mK}$  in simulation one and elevated by a factor 100 in simulation two. The results showed no effect of the mass flow rate what so ever.

Viscosity were held constant throughout the simulations. This might effect the result but to what extent has not been investigated.

Even though this work indents to simulate a real throttle body and intake manifold on an actual engine there are things that for different reasons has been approximated. The purpose has been to establish trends and behaviour of certain properties not to duplicate the results from engine measurements with simulations. The flow is considered stationary, simulating instationary gas flow would be desirable but are very computer demanding. The simulated geometry differs from the actual one, for example the throttle body cross section is a perfect circle in simulations the actual one is an ellipse. The walls in the simulated geometry are perfectly smooth or have the same sand-grain roughness. This will make the results from simulations differ from engine measurements. If there were possibilities to replicate the exact engine measurements with simulations one must keep in mind that the results only apply to that specific engine. By studying a more general throttle body and intake manifold and comparing behaviour instead of exact values a broader understanding to why the flow is choked at a certain point hopefully is gained.



# Chapter 5

## Analysis

### 5.1 Ways of Comparison

There are more than one way to compare differences between the simulations. In this work the ways of comparison have been divided into three subgroups.

- Global level, which compares total mass and heat flux.
- Local level, compare heat fluxes for each part, throttle body, shaft, edge etc.
- Node level, compare velocities, pressure, density etc. at each computational node.

The global level has been of main interest since it gives direct scalar values without any post processing. By comparing the mass flow rate the influence of the studied assumption has been estimated. To visualize local differences between the simulations the following method where used. From a plane in line with the throttle body center axis and the throttle shaft as normal, data at each node were extracted.

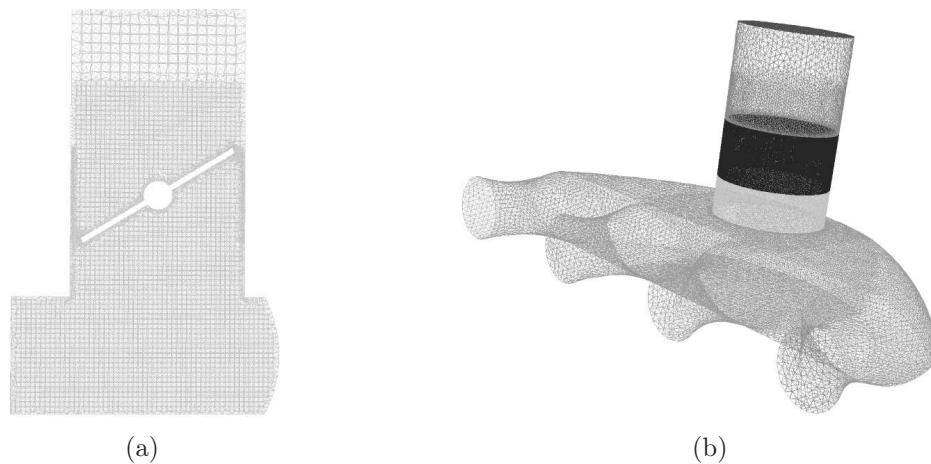


Figure 5.1: **(a)** Example of a plane computational grid. **(b)** Complete exterior grid visual.

Let  $q_1(i, j)$  and  $q_2(i, j)$  be values of a studied variable in the plane from each simulation. To compare the differences between  $q_1$  and  $q_2$  they were subtracted from one another forming a new set of values  $f(i, j)$

$$f(i, j) = q_1(i, j) - q_2(i, j) \quad (5.1)$$

The new set of values  $f$  describes the difference at each node. Let the circles in figure 5.2 represent a value at a specific node  $f(i, j)$ .

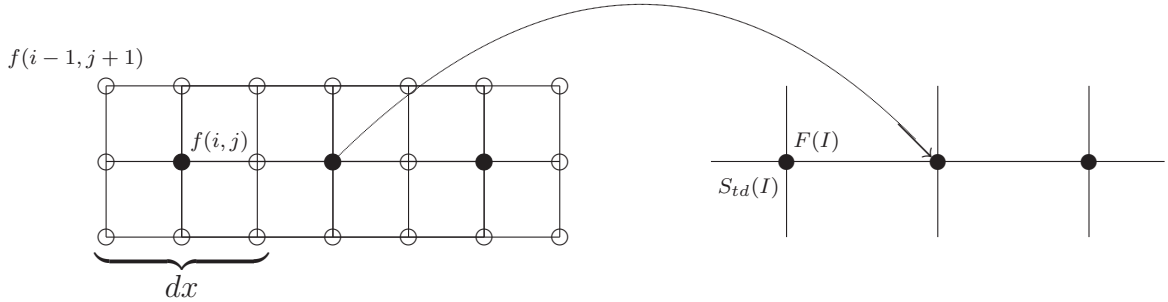


Figure 5.2: Example of grid used to downsample and calculate mean value and standard deviation.

For every interval  $dx$  the mean value  $F(I)$  and the standard deviation  $S_{td}(I)$  are calculated.

$$F(I) = \frac{1}{N_{ndx}} \sum_{m=j-1}^{j+1} \sum_{k=i-1}^{i+1} f(k, m) \quad N_{ndx} = \text{Number of nodes in interval } dx \quad (5.2)$$

$$S_{td}(I) = \sqrt{\frac{1}{N_{ndx}} \sum_{m=j-1}^{j+1} \sum_{k=i-1}^{i+1} (f(k, m) - F(I))^2} \quad (5.3)$$

In addition to this there are numerous ways to visualize results in FLUENT, contours, vectors, pathlines etc.

## 5.2 Estimating Effects of Wall Heating

The temperatures which the throttle body has to operate at is far from constant. At engine start up the throttle body has approximately the same temperature as the surrounding air. The engine will then gradually reach its working temperature which is in the area of  $85 - 95^\circ C$ . Simulations were ran with external and internal wall temperatures at  $358 K$  ( $85^\circ C$ ) to ascertain what effect a heated wall will have in comparison with an adiabatic. A total of 12 simulations were calculated, six at throttle angle  $31^\circ$ , six at a throttle angle  $21^\circ$ . The pressure ratios were set to 0.2, 0.4 and 0.6 for each throttle angle. As references simulations were conducted at the same pressure

ratios and throttle angles with adiabatic and smooth walls. The amount of heat per mass fluid transferred from the intake manifold, throttle - plate, shaft, body and edge has been calculated by summarizing the heat flows through the particular parts and dividing with the mass flow rate.

$$\frac{W}{\dot{m}} = \frac{J}{kg} \quad (5.4)$$

### 5.3 Estimating Effects of Wall Surface Roughness

Pressure losses caused by wall surface roughness is in this particular case hard to measure due to the experimental setup. There are however possibilities to simulate surface roughness using FLUENT. There are two parameters when modeling wall roughness in FLUENT, the roughness height  $K_s$  and roughness constant  $C_s$ . The roughness height constant can be chosen as the sand-grain roughness height thus assuming uniform sand-grain roughness [6]. Modeling the actual wall roughness has been seen as too difficult and the main interest is the effect of wall roughness not to model the true nature of the walls in a real intake manifold. The choice of  $K_s$  has been done by taking three things in concern. The inlet pipe which in the real engine is a braided rubber hose, the throttle body itself which has a somewhat machined smooth surface and the intake manifold which is sand-casted. For newly cast pipes  $K_s$  ranges from 0.2 – 0.6 mm. When simulating wall roughness  $K_s$  has been set at 0.2 mm, assuming that the inlet pipe and throttle body has similar wall roughness as the intake manifold. The roughness constant  $C_s$  was set to its default value of 0.5. The default value was determined so when used with the  $k - \epsilon$  turbulence model it would replicate Nikuradse's resistance data for pipes with uniform sand-grain roughness [6]. As for wall heating a total of 12 simulations were ran, six at throttle angle 31°, six at a throttle angle 21°. The pressure ratios were set to 0.2, 0.4 and 0.6. For each throttle angle three simulations were used as references which had smooth and adiabatic walls. To evaluate what influence each part had the wall shear stress  $\tau_w$  were integrated over the surface area for each part, intake manifold throttle plate, shaft and edge and the throttle body itself.

$$\int \tau_w dA \quad (5.5)$$

The wall shear stress can be simplified using a laminar zone close to the wall and is defined by the normal velocity gradient at the wall.

$$\tau_w = \mu \frac{\partial v}{\partial n} \quad (5.6)$$

## 5.4 Calculating the Effective Flow Area

The discharge coefficient  $C_d$  is somewhat of a gray area. When discussing  $C_d$  one must be very careful describing what definition is used. In section 3.1.3 there are multiple ways to describe the discharge coefficient and a proper explanation of which model that is being used must be defined before any conclusions are made. As with all experiments determining  $C_d$  the results from the simulations are only valid for the specific geometry and not applicable for others. It might give an indication of how the flow is affected of a certain geometry but never precise values. As stated in section 3.1.3 one can write the coefficient of discharge as,

$$C_{d_{is}} = \frac{\text{effective throat area}}{\text{geometrical throat area}} = \frac{A_{te}}{A_g} \quad (3.17)$$

It is commonly known that air flow will contract after an orifice forming a cross sectional area smaller then the geometrical one<sup>1</sup> the phenomena is sketched in figure 5.3. The phenomena have also been observed in the simulations as seen in figure 5.4(b). It where of great interest to calculate the effective area and put in correlation to the mass flow rate.

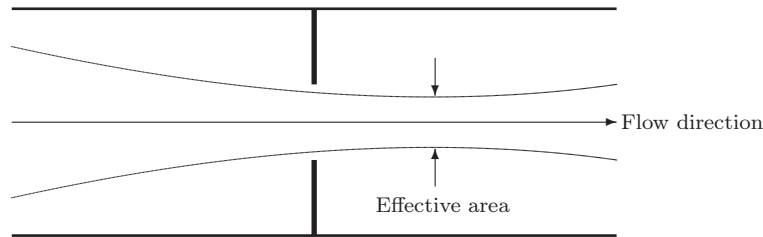


Figure 5.3: Vena contracta forming after the minimum geometric cross sectional area.

By releasing pathlines from the throttle edge, figure 5.4(a) and calculate the perpendicular distance to the center axis of the throttle body a method has been constructed to establish the effective area.

The following steps describe the algorithm.

Let  $P(x, y, z)_n$  be the position of a massless particle released from the throttle edge. The coordinate system is located in such a way that the  $y$  - axis is located in the center of the throttle body pointing toward the inlet. The perpendicular distance to the  $y$  - axis,  $P_d$  is calculated by

$$P_d(x, y, z)_n = \sqrt{P(x, y, z)_n \cdot P(x, 0, z)_n} \quad n = 1, 2 \dots \text{number of particles.} \quad (5.7)$$

For every  $P_d(x, y, z)_n$  the maximum distance to the center axis is calculated.

$$P_{d_{max}}(x, y, z)_n = \max \{P_d(x, y, z)_n\} \quad (5.8)$$

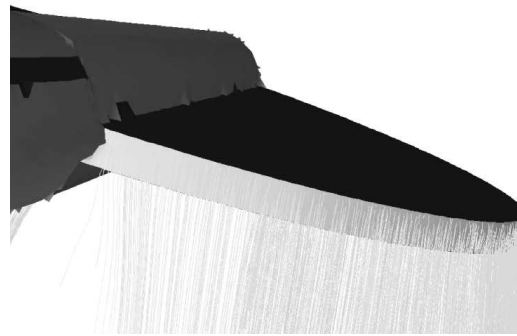
<sup>1</sup>The smaller cross sectional area or effective area is known as vena contracta

By using this method the area can be described and visualized in 3 dimensions, figure 5.5. The max value point acquired for each pathline is projected on the x-z plane and enclosed by the MATLAB function *convhull*, figure 5.6(a). Finally the area can be calculated by using MATLAB function *polyarea*, figure 5.6(b). The coefficient of discharge has been calculated in two ways, one based on mass flow rate and one on effective area.

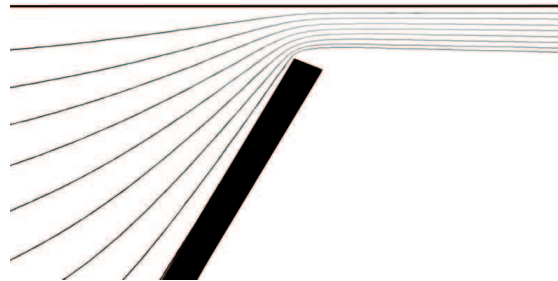
$$C_{disentropic} = \frac{\dot{m}_{simulated}}{\dot{m}_{isentropic}} \quad (5.9)$$

$$C_{d_{area}} = \frac{A_{te}}{A_g} \quad (5.10)$$

The isentropic mass flow rate is calculated by equation 2.22 on page 9. The effective area is calculated by the method previously described. The geometrical area  $A_g$  has been calculated in FLUENT by projecting the throttle - shaft, plate and edge on the x-z plane.



(a)



(b)

Figure 5.4: (a) Pathlines releasing from throttle plate edge used to calculate the effective area. (b) Pathlines showing a contraction behind the throttle plate forming the effective area.

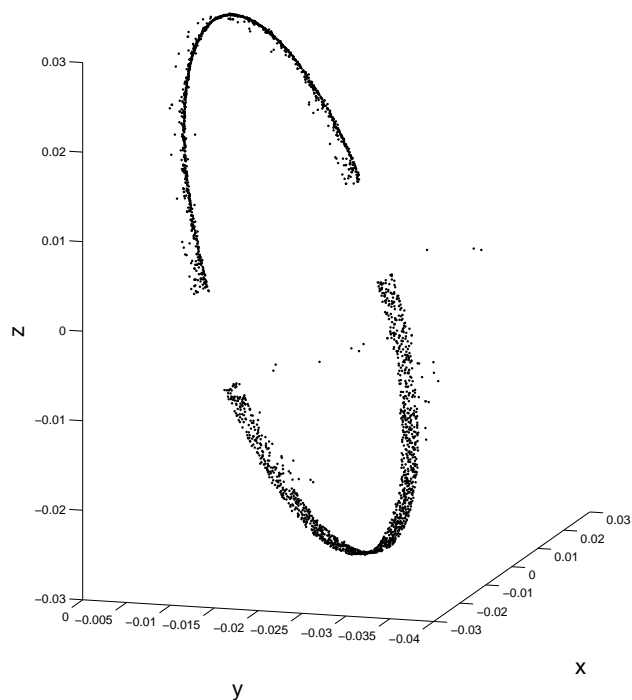


Figure 5.5: 3D scatter plot of the points used to calculate the effective area.

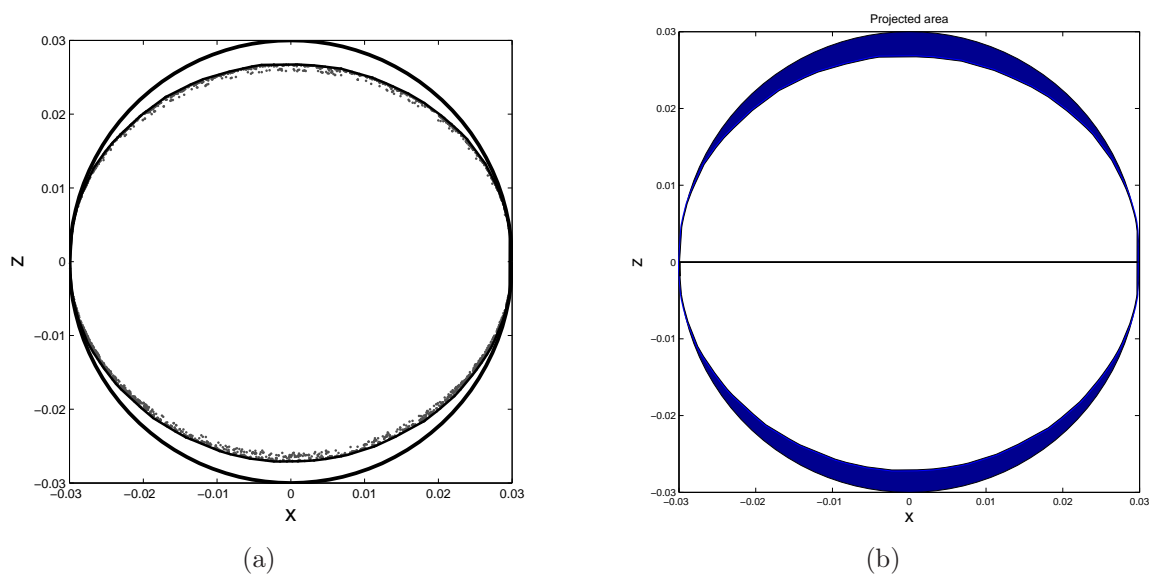


Figure 5.6: **(a)** Scatter plot of points with maximum distance to center axis projected on the x-z plane enclosed with MATLAB function *convhull*. **(b)** Filled area with MATLAB function *polyarea*



## 5.5 Results

### Effects of wall heating.

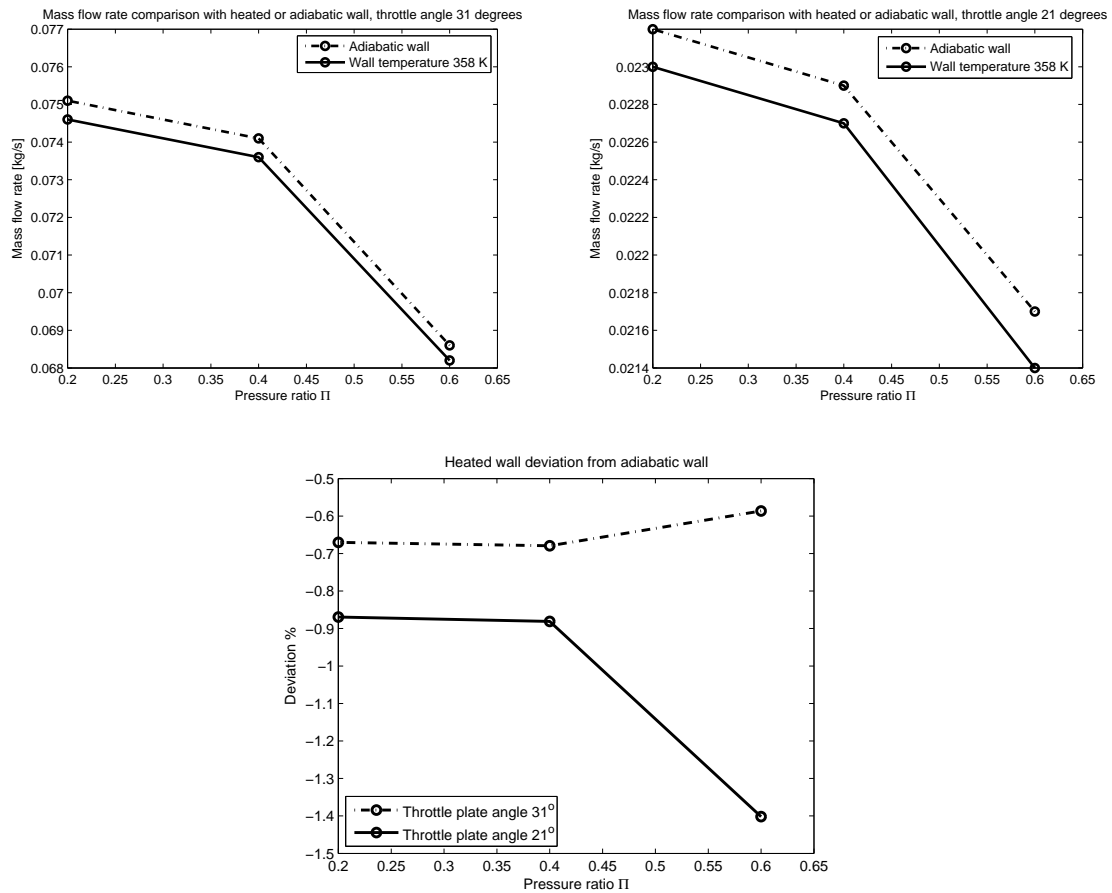


Figure 5.7: Mass flow rate and deviation from an adiabatic wall when investigating the influence of a heated wall. *Top*: Mass flow rate (observe the scale) at throttle plate angle, *left*: 31°, *right*: 21°. *Bottom*: Deviation from adiabatic wall.

Throttle plate angle	$\alpha = 31^\circ$			$\alpha = 21^\circ$		
Pressure ratio	0.2	0.4	0.6	0.2	0.4	0.6
Heat Transfer Rate [W]	1277	1377	1346	647	683	669
Mass flow rate $\left[\frac{kg}{s}\right]$	0.0746	0.0736	0.0682	0.0230	0.0227	0.0214
Heat quota $\left[\frac{J}{kg}\right]$	17117	18697	19735	28166	30138	31217

Table 5.1: Heat transferred through walls and by the throttle - plate, edge and shaft

Effects of surface roughness.

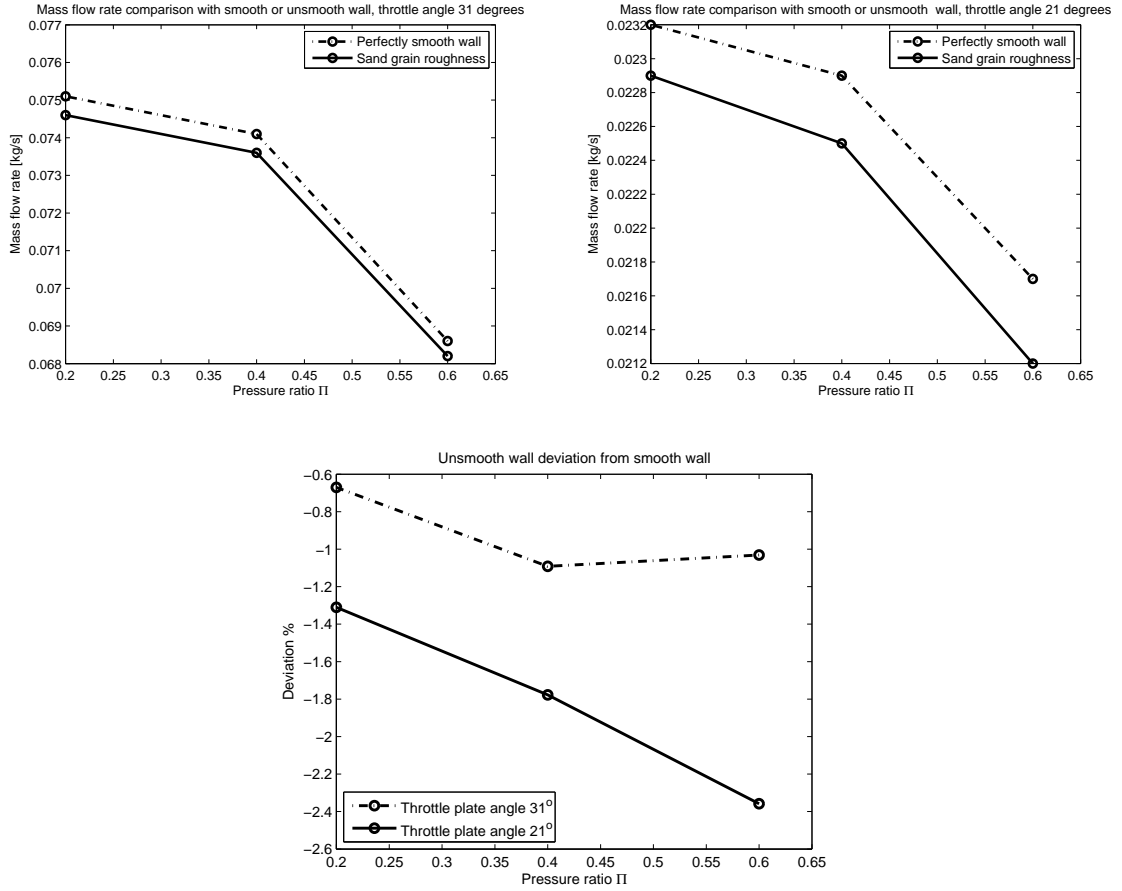


Figure 5.8: Mass flow rate and deviation from a smooth wall when investigating the influens wall surface roughness. *Top*: Mass flow rate (observe the scale) at throttle plate angle, *left*: 31°, *right*: 21°. *Bottom*: Deviation from smooth wall.

	Throttle plate angle	$\alpha = 31^\circ$			$\alpha = 21^\circ$		
	Pressure ratio II	0.2	0.4	0.6	0.2	0.4	0.6
$\int \tau_w dA$	Throttle body wall	2.44	2.63	2.09	1.74	1.59	1.18
	Throttle plate	0.12	0.11	0.09	0.05	0.04	0.04
	Throttle edge	0.17	0.15	0.10	0.18	0.17	0.13
	Throttle shaft	0.012	0.012	0.01	0.01	0.004	0.003
	Intake manifold	3.47	2.71	1.78	0.91	0.68	0.44

Table 5.2: Integrated wall shear stress for each part when investigating the influence of wall surface roughness

## Coefficient of discharge.

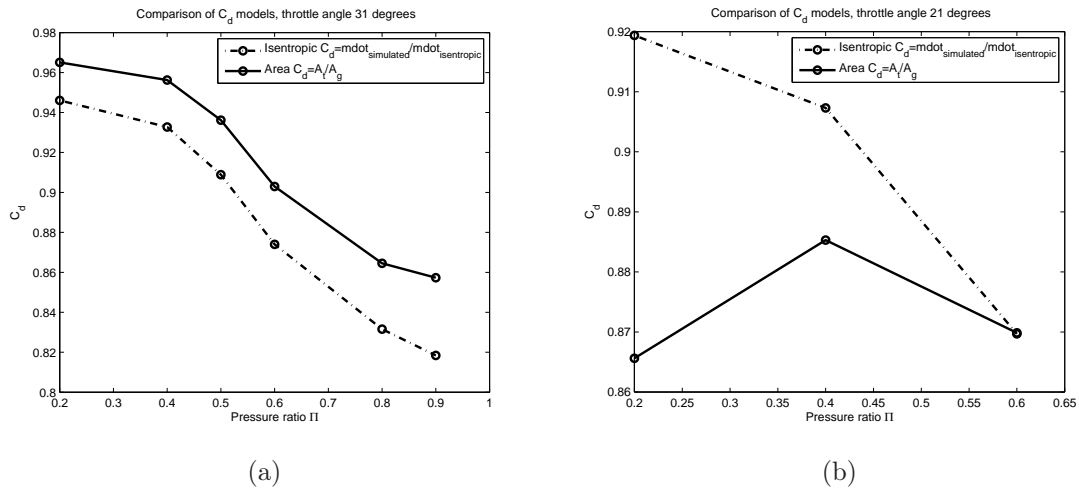


Figure 5.9: Coefficient of discharge calculated and measured with FLUENT, solid line represent  $C_{d_{area}}$  and dotted  $C_{d_{isentropic}}$ . (a) Throttle angle =  $31^\circ$ . (b) Throttle angle =  $21^\circ$

## 5.6 Discussion

### 5.6.1 Mesh Generation

The mesh generation process is somewhat arbitrary. The cells near the throttle edge must be substantially small to get high resolution at the restriction. The process presents a challenge to get a mesh with good quality and substantial number of cells in conflict with computer performance. Multiple meshes were designed with different mesh density to achieve high quality. This however gave an opportunity to check the mesh independence for the different mesh densities. The different mesh sizes were simulated with a smooth and adiabatic wall at a pressure ratio of  $\Pi = 0.6$ , the mesh in all cases consists of unstructured tetrahedral cells.

Number of cells	Mass flow rate $\frac{kg}{s}$	Percentage deviation from densest grid
557 000	0.0695	1.3 %
800 000	0.0694	1.2 %
1 300 000	0.0689	0.4 %
2 700 000	0.0686	0 %

Table 5.3: Number of cells and mass flow rate in geometry, mesh independence check.

### 5.6.2 Wall Heat

Heat addition from the wall has showed an effect on the flow dependent on both throttle plate angle and pressure ratio, figure 5.7. It has showed that the mass flow rate will be effected more at the smaller throttle plate angle  $21^\circ$  than  $31^\circ$ . If this behaviour increases for even smaller throttle plate angles the deviation from the adiabatic will of course also be greater. One can probably expect that the effect increases with smaller throttle plate angles due to the fact that the fluid will spend more time in the geometry, caused by the lower mass flow rate.

The two throttle plate angles both show a decrease of mass flow rate but the deviation from the adiabatic wall used as reference does not follow the same pattern. The larger mass flow rate will result in a larger heat transport however the amount of heat per mass fluid will increase with smaller mass flow rate, that is, the quota  $\frac{W}{\dot{m}} = \frac{J}{kg}$  will be greater for smaller mass flow rates. Why the heat transfer rate is greater for larger throttle plate angle may be explained by following empirical expression.

$$\dot{Q} = A\alpha'(T_w - T_f) \quad (5.11)$$

Where  $\alpha'$  is the heat transfer coefficient and  $A$  is the area which the heat flux passes. The heat transfer coefficient will be greater for larger mass flow rates caused by an increased velocity close to the wall. Still, more heat per mass of fluid will be transferred to the flow at the smaller throttle plate angle resulting in an elevated temperature of the fluid as can be seen in figure 5.10. This in turn results in an decrease of mass flow rate.

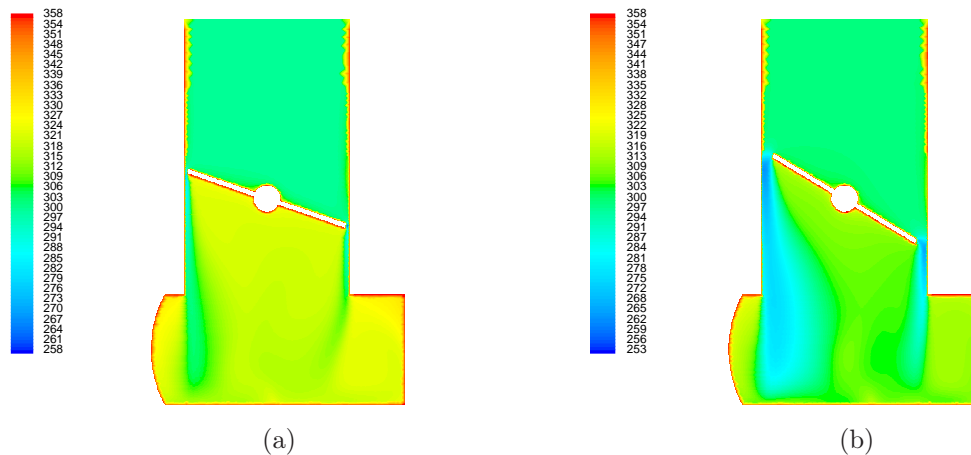


Figure 5.10: Static temperature field in K,  $\Pi = 0.6$ , wall temperature 358 K. (a): 21 degrees of throttle plate angle, (b): 31 degrees of throttle plate angle.

One should keep in mind that the simulations were conducted at steady state. Unsteady, pulsating flow has showed to double the heat transfer rate compared with stationary flow [2].

### 5.6.3 Wall Surface Roughness

If one compares the integrated wall shear stress it is a clear shift in which part that have the largest influence on the flow when comparing the two different angles, table 5.2. For the larger throttle plate angle the intake manifold have the most influence. At the smaller angle this have shifted to the throttle body wall. The throttle edge has even higher wall shear stress for the smaller throttle plate angle. One plausible explanation to this is that at the smaller throttle plate angle the flow will be forced closer to the wall thus increasing the velocity gradient. Even if the throttle plate angle is decreased or increased the highest velocity at the throat is mainly pressure ratio dependent see equation 2.22, the velocities close to the wall in the intake manifold is mass flow rate dependent caused by the low pressure gradients in the intake manifold. This could explain why this shift happens. As with wall heating the effect from wall surface roughness is both pressure ratio and throttle plate angle dependent, figure 5.8.

### 5.6.4 Effective Area

From simulations it has been concluded that for 31° of throttle plate angle  $C_{d_{area}}$  is larger than  $C_{d_{isentropic}}$ , see figure 5.9(a). Viscous and turbulence effects may explain the deviation. The behaviour is however almost the same. For 21° of throttle plate angle the behaviour is completely different, figure 5.9(b). At the lower pressure ratio  $C_{d_{area}}$  even showed a decrease. At the smaller angle wall attachment effects and the boundary layer play a more dominant role of the flow, this or numerical deviations might explain

the behaviour. One should keep in mind that the largest perpendicular distance from the throttle edge to the throttle body wall at this angle is about 2 mm.

In this report the effective area is defined as the minimum cross sectional area between the throttle body wall and the artificial boundary which particles released from the throttle edge would generate, see section 5.4. This definition or model is one of many ways to describe the effective area. It has been seen that the behaviour of the mass flow rate coincide with the effective area, at least for 31° of throttle plate angle. This leads one to believe that the model is sufficiently good.

For 31° of throttle plate angle one possible answer to how the effective area changes with pressure ratio is that the effective area restrict the mass flow rate but in it self it has no capability to actually choke the flow. When Mach one is achieved in the geometrical area the pressure ratio can be decreased without any increase in mass flow rate and so the flow is choked. As pressures ratio is decreased the effective area gets closer to the geometrical one and at specific pressure ratio  $\Pi_{choked}$  the two will coincide.

$$\lim_{\Pi \rightarrow \Pi_{choked}} C_{d_{area}} = 1 \quad (5.12)$$

This may also explain why the flow is choked at a lower pressure ratio than the isentropic model. The effective area is not an actual boundary merely an artificial created by the nature of the flow. The calculated isentropic critical pressure ratio where the flow reaches Mach one is correct if one expects it in the effective area however mass flow rate will continue to increase to that point where Mach one is obtained in the entire geometrical restriction.

If an isentropic model is used to describe the flow past the throttle plate and the discharge coefficient is used as a curve adjustment parameter it should be noticed that  $C_d$  is a measurement of how much the actual flow differs from the isentropic one and not a proper representation of how the effective area differs from geometrical.

It has been observed Mach numbers exceeding one after the throttle edge, figure 5.12 which indicates that the pressure field in cooperation with the throttle plate edge acts as an convergent-divergent nozzle. To what extent this is possible or not is hard to validate with engine measurements but one can probely expect it at some throttle angles which intensifies the effect. The phenomenon is sketched in figure 5.11, it is likely that shock waves occurs when the flow i decelerated from  $M > 1$  to  $M \leq 1$ .

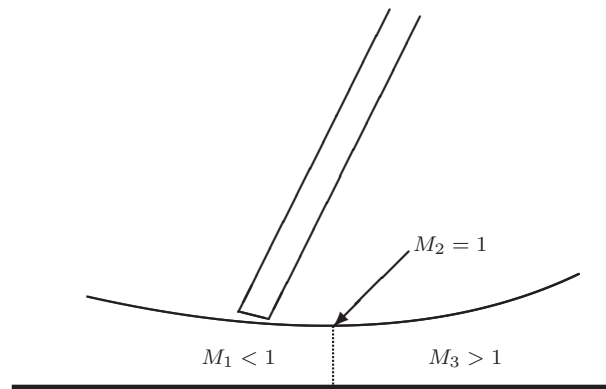


Figure 5.11: Convergent - divergent nozzle forming downstream throttle edge

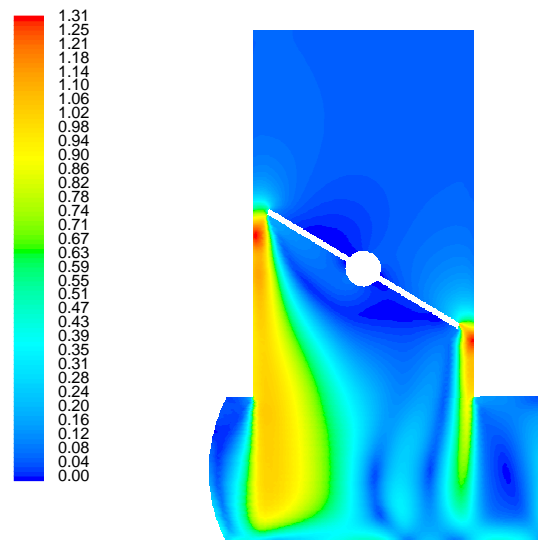


Figure 5.12: Mach number exceeding one after the throttle plate

What influence the turbulence model had on the results must be determined by simulating with other models. However the greatest deviation from reality is probably done by assuming stationary flow. Investigating instationary flow caused by intake valves opening and closing before testing different turbulence models seems as the natural step to continue this work.

## 5.7 Conclusions

Both wall heating and wall surface roughness will reduce the mass flow rate compared to an adiabatic or perfectly smooth wall. Similar effects have been found when studying converging nozzles [11]. By simulations it has been concluded that the wall itself plays an important part of the flow, two throttle plate angles were studied, a clear throttle plate angle and pressure ratio dependence can be observed. It is without problem easy to adjust the isentropic throttle model used for engine simulations to fit engine measurements. However to gain a greater understanding of the flow it is important to recognize that there are several parameters that affect the flow and reducing all of them to the effective area may be to cut corners. In addition to this comes effects from swirl in the inlet caused by the ducts leading from the intercooler or air filter that has not been studied in this report.



# Chapter 6

## Nomenclature

Symbol	Description	Unit
$\alpha$	Throttle plate angle	[ $^{\circ}$ ]
$\alpha'$	Convection heat transfer coefficient	[ $\frac{W}{m^2K}$ ]
$\alpha_0$	Throttle plate rest angle	[ $^{\circ}$ ]
$\alpha_1$	Fitting constant	
$\alpha_2$	Fitting constant	
$\epsilon$	Turbulent dissipation rate	[ $\frac{m^2}{s^3}$ ]
$\gamma$	Ratio of specific heat $\frac{c_p}{c_v} = 1.4$	
$\lambda$	Second viscosity coefficient	[ $\frac{kg}{ms}$ ]
$\mu$	Molecular viscosity coefficient	[ $\frac{kg}{ms}$ ]
$\Pi$	Pressure ratio	
$\Pi_{crit}$	Critical pressure ratio	
$\rho$	Density	[ $\frac{kg}{m^3}$ ]
$\tau$	Shear stress	[ $Pa$ ]
$a$	Local speed of sound	[ $\frac{m}{s}$ ]
$A_g$	Geometrical area	[ $m^2$ ]
$A_{te}$	Effective area	[ $m^2$ ]
$C_d$	Coefficient of discharge	
$c_p$	Specific heat capacity, constant pressure	$\frac{J}{kgK}$
$c_v$	Specific heat capacity, constant volume	$\frac{J}{kgK}$
$C_{\mu}$	Emperical constant, value $\approx 0.09$	
$D$	Throttle body diameter	[ $mm$ ]
$e$	Internal energy	[ $\frac{kJ}{kg}$ ]
$h$	Enthalpy	[ $\frac{kJ}{kg}$ ]
$I$	Turbulence Intensity	[ $\%$ ]
$k$	Thermal conductivity	[ $\frac{W}{mK}$ ]
$K_s$	Roughness height	[ $mm$ ]
$\ell$	Turbulence Length Scale	[ $m$ ]
$M$	Mach number	
$\dot{m}$	Mass flow rate	[ $\frac{kg}{s}$ ]
$\dot{m}_{at1}$	Fitting constant	

Symbol	Description	Unit
$\dot{m}_{ex}$	Actual mass flow rate	$[\frac{kg}{s}]$
$\dot{m}_{is}$	Isentropic mass flow rate	$[\frac{kg}{s}]$
$p_1$	Pressure before throttle plate	$[Pa]$
$p_2$	Pressure after throttle plate	$[Pa]$
$p'_1$	Fitting constant	
$p'_2$	Fitting constant	
$p_{after}$	Pressure after throttle plate	$[Pa]$
$p_{before}$	Pressure before throttle plate	$[Pa]$
$p_a$	Pressure in front of throttle plate	$[Pa]$
$p_i$	Manifold pressure	$[Pa]$
$\dot{q}$	Heat flux	$[\frac{W}{kg}]$
$\dot{Q}$	Heat flux rate	$[W]$
$t$	Throttle plate thickness	$[mm]$
$T_1$	Temperature before throttle plate	$[K]$
$T_2$	Temperature after throttle plate	$[K]$
$T_{after}$	Temperature after throttle plate	$[K]$
$T_{before}$	Temperature before throttle plate	$[K]$
$T_w$	Temperature of wall	$[K]$
$T_f$	Temperature of fluid	$[K]$
$R$	Ideal gas constant	$[\frac{J}{kgK}]$
$Re$	Reynold number	
$u$	Velocity, x-direction	$[\frac{m}{s}]$
$u_{avg}$	Mean flow velocity	$[\frac{m}{s}]$
$v$	Velocity, y-direction	$[\frac{m}{s}]$
$w$	Velocity, z-direction	$[\frac{m}{s}]$
$\mathbf{V}$	Vector velocity	$[\frac{m}{s}]$

# Bibliography

- [1] Per Andersson. *Air Charge Estimation in Turbocharged Spark Ignition Engines*. Ph.D. dissertation., Dept. of Electrical Engineering Linköping University, Linköping, Sweden, 2005. Linköping Studies in Science and Technology Thesis No. 989.
- [2] Wolf-D. Bauer, Joseph Wenisch, and John B. Heywood. Averaged and time-resolved heat transfer of steady and pulsating entry flow in intake manifold of a spark-ignition engine. *International Journal of Heat and Fluid Flow* 19(1998)1-9, 1997.
- [3] Gordon P. Blair. *Design and simulation of four-stroke engines*. Warrendale, PA : Society of Automotive Engineers, 1999. ISBN 0768004403.
- [4] Yunus A. Çengel and Robert H. Turner. *Fundamentals of Thermal-Fluid Sciences*. McGraw-Hill Book Company, 2001. ISBN 0-07-239054-9.
- [5] John D. Anderson. *Computational Fluid Dynamics, The basics with applications*. McGraw-Hill Book Company, 1995. International Edition.
- [6] Fluent Inc. *FLUENT 6.1 User's Guide*, February 2003.
- [7] Elbert Hendricks, Alain Chevalier, Michael Jensen, and Spencer C Sorenson. Modelling of the intake manifold filling dynamics. *SAE Technical Paper No. 960037*, 1996.
- [8] John B. Heywood. *Internal Combustion Engine Fundamentals*. McGraw-Hill Book Company, 1988. ISBN 0-07-100499-8.
- [9] H-D Kim, J-H Kim, K-A Park, T setoguchi, and S Matsuo. Computational study of gas flow through a critical nozzle. In *Proceedings of the Institution of Mechanical Engineers*, volume 217. School of Mechanical Engineers, 2003. Part C.
- [10] Mattias Kryssander. Airflow past a throttle plate. Master's thesis, University of Linköping, 2000.
- [11] A Alper Ozalp. Numerical analysis of choked converging nozzle with surface roughness and heat flux conditions. *Sadhana - Academy Proceedings in Engineering Sciences* 31 (1), pp. 31-46, 2006.
- [12] Ross Pursifull, Alain J. Kotwiski, and Sulgi Hong. Throttle flow characterization. *SAE Technical Paper No. 2000-01-0571*, 2000.



# Appendix A

## Results in Tabular Form

Throttle plate angle	Pressure ratio II	Wall property	Mass flow rate $\frac{kg}{s}$
$\alpha = 31^\circ$	0.6	Adiabatic	0.0686
	0.4	Adiabatic	0.0741
	0.2	Adiabatic	0.0751
	0.6	358 K	0.0682
	0.4	358 K	0.0736
	0.2	358 K	0.0746
$\alpha = 21^\circ$	0.6	Adiabatic	0.0217
	0.4	Adiabatic	0.0229
	0.2	Adiabatic	0.0232
	0.6	358 K	0.0214
	0.4	358 K	0.0227
	0.2	358 K	0.0230

Table A.1: Mass flow rate when investigating the influence of wall heating

Throttle plate angle	Pressure ratio II	Wall property	Mass flow rate $\frac{kg}{s}$
$\alpha = 31^\circ$	0.6	Smooth	0.0686
	0.4	Smooth	0.0741
	0.2	Smooth	0.0751
	0.6	$K_s = 0.2 \text{ mm}$	0.0679
	0.4	$K_s = 0.2 \text{ mm}$	0.0733
	0.2	$K_s = 0.2 \text{ mm}$	0.0746
$\alpha = 21^\circ$	0.6	Smooth	0.0217
	0.4	Smooth	0.0229
	0.2	Smooth	0.0232
	0.6	$K_s = 0.2 \text{ mm}$	0.0212
	0.4	$K_s = 0.2 \text{ mm}$	0.0225
	0.2	$K_s = 0.2 \text{ mm}$	0.0229

Table A.2: Mass flow rate when investigating the influence of wall surface roughness

Throttle plate angle	Pressure ratio $\Pi$	Mass flow rate $\frac{kg}{s}$	$C_{d_{area}}$	$C_{d_{isentropic}}$
$\alpha = 31^\circ$	0.9	0.0401	0.86	0.82
	0.8	0.0541	0.86	0.83
	0.6	0.0686	0.90	0.87
	0.5	0.0722	0.94	0.91
	0.4	0.0741	0.96	0.93
	0.2	0.0751	0.97	0.95
$\alpha = 21^\circ$	0.6	0.0217	0.87	0.87
	0.4	0.0229	0.89	0.91
	0.2	0.0232	0.87	0.92

Table A.3: Mass flow rate and coefficients of discharge.  $C_{d_{area}}$  is calculated by measuring the effective area with the method presented in section 5.4,  $C_{d_{area}} = \frac{A_{te}}{A_g}$ ,  $C_{d_{isentropic}} = \frac{\dot{m}_{simulated}}{\dot{m}_{isentropic}}$ .

# Appendix B

## MATLAB Code

### reader.m

Extracts data from path line files.

```
0 function [xout,yout] = reader(fname,ncols,nhead,particles)
1 %Syntax [xout,yout] = reader(fname,ncols,nhead,particles)
2 %fname = filename
3 %ncols = 2;
4 %nhead = Number of lines to skip in begining of file or in middle
5 %particles= Number of repeating systems
6 % Example, if fname=
7 %     [aaaaaa
8 %     1  2
9 %     3  4
10 %     bbbbb
11 %     1  3
12 %     4  1]
13 % The call to reader will be
14 %[xout,yout] = reader(fname,2,1,2)
15 %
16 %Per Carlsson, Linköping 2006-11-21
17
18
19 fin = fopen(fname,'r');
20
21 if fin < 0
22     error(['Could not open ',fname,' for input']);
23 end
24
25 for count=1:particles
26
```

```
27 for i=1:nhead,
28     buffer = fgetl(fin);
29 end
30
31 data = fscanf(fin,'%f');
32
33 nd = length(data);
34 nr = nd/ncols;
35 data = reshape(data,ncols,nr)';
36 x = data(:,1);
37 y = data(:,2:ncols);
38
39
40 xout(1:length(x),count)=x;
41 yout(1:length(y),count)=y;
42
43 end
44 fclose(fin);
```



---

## distxyz.m

Calculates the distance to the center axis of the throttle body.

```
0  clear all
1  close('all')
2  clc
3
4  pressure_ratio='05';
5
6  numpath=3000;           %Number of pathlines
7  t=1;                   %Counter
8
9  filenamex=['xpath',pressure_ratio]; %file with x-values
10 filenamey=['ypath',pressure_ratio]; %file with y-values
11 filenamez=['zpath',pressure_ratio]; %file with z-values
12
13 %%%%%%%%%%%%%%%%%%%%%%%%%%%%%%%%%%%%%%%%%%%%%%%%%%%%%%%%%%%%%%%%%%%%%%%%%
14 %Loads data from the files
15
16 disp('Reading files')
17 [pathx,distx]=reader(filenamex,2,3,numpath);
18 [pathy,disty]=reader(filenamey,2,3,numpath);
19 [pathz,distz]=reader(filenamez,2,3,numpath);
20 disp('Done reading')
21
22 %Calculate maximum distance from centerline.
23 for i=1:numpath
24
25     if sum(distx(:,i))==0 |sum(disty(:,i))==0 |sum(distz(:,i))==0
26         break
27         disp('break')
28     end
29
30     if t==100
31         disp(' ')
32         disp(['Processing pathline number: ' num2str(i)])
33         t=0;
34     end
35
36     xyz_dist(:,1,i)=distx(:,i);
37     xyz_dist(:,2,i)=disty(:,i);
38     xyz_dist(:,3,i)=distz(:,i);
39     xyz_dist(:,4,i)=sqrt(distx(:,i).^2+distz(:,i).^2);
40     t=t+1;
41 end
```

```
42
43 [row col dep]=size(xyz_dist);
44
45 for q=1:dep
46
47     sort=sortrows(xyz_dist(:,:,q),4);
48     maxdist(q,:)=sort(end,:);
49 end
50
51 %Displays results
52 %*****
53 figure(1)
54 plot(maxdist(:,1),maxdist(:,3),'.k')
55
56 x=maxdist(:,1);
57 y=maxdist(:,3);
58
59 k=convhull(x,y);
60
61 hold on
62 plot(x(k),y(k),'-', 'linewidth',3)
63 wall = rsmak('circle',0.03);
64
65 points=fnplt(wall,'k');
66 fnplt(wall,'k')
67 set(gca,'DataAspectRatio',[1 1 1])
68
69 xp=points(1,:);
70 yp=points(2,:);
71
72 geoproj=106.0298882
73 % 333.5206882, 31 degrees ;
74 totarea=0.03^2*pi*1000000;
75 tharea=totarea-polyarea(x(k),y(k))*1000000;
76 Codis=tharea/geoproj;
77
78 at=['Projected area from Fluent = ' num2str(geoproj) ' mm^2'];
79 ag=['Throated area = ' num2str(tharea) ' mm^2'];
80 coefd=['Coefficient of discharge = ' num2str(Codis)];
81 P_ratio=['Pressure ratio = ',pressure_ratio];
82 tit={at; ag;coefd;P_ratio};
83 title(tit)
84 xlabel('x','FontSize',18)
85 ylabel('z','FontSize',18)
86
87 hold off
```

---

```
88 %*****
89 figure(2)
90 plot3(maxdist(:,1),maxdist(:,2), maxdist(:,3),'.k')
91 hold on
92 set(gca,'DataAspectRatio',[1 1 1])
93 xlabel('x','FontSize',18)
94 ylabel('y','FontSize',18)
95 zlabel('z','FontSize',18)
```



**LINKÖPINGS UNIVERSITET**

**Avdelning, Institution**  
Division, Department

Applied Thermodynamics and Fluid  
Mechanics, IEI.

**Datum**  
Date

February 23, 2007

**Språk**

Language

- Svenska/Swedish  
 Engelska/English

\_\_\_\_\_

**Rapporttyp**

Report category

- Licentiatavhandling  
 Examensarbete  
 C-uppsats  
 D-uppsats  
 Övrig rapport  
 \_\_\_\_\_

**ISBN**

**ISRN**

LIU-IEI-TEK-A-07/0071-SE

**Serietitel och serienummer ISSN**

Title of series, numbering

**URL för elektronisk version**

<http://urn.kb.se/resolve?urn=urn:nbn:se:liu:diva-8378>

**Titel**  
Title

Flow Through a Throttle Body. A Comparative Study of Heat Transfer, Wall Surface  
Roughness and Discharge Coefficient.

**Författare**  
Author

Per Carlsson

**Sammanfattning**

Abstract

When designing a new fuel management system for a spark ignition engine the amount of air that is fed to the cylinders is highly important. A tool that is being used to improve the performance and reduce emission levels is engine modeling where a fuel management system can be tested and designed in a computer environment thus saving valuable setup time in an engine test cell. One important part of the modeling is the throttle which regulates the air. The current isentropic model has been investigated in this report. A throttle body and intake manifold has been simulated using Computational Fluid Dynamics (CFD) and the influence of surface heating and surface wall roughness has been calculated. A method to calculate the effective flow area has been constructed and tested by simulating at two different throttle plate angles and several pressure ratios across the throttle plate. The results show that both surface wall roughness and wall heating will reduce the mass flow rate compared to a smooth and adiabatic wall respectively. The reduction is both dependent on pressure ratio and throttle plate angle. The effective area has showed to follow the same behaviour as the mass flow rate for the larger simulated throttle plate angle 31°, i.e. an increase as the pressure drop over the throttle plate becomes larger. At the smaller throttle plate angle 21°, the behaviour is completely different and a reduction of the effective area can be seen for the highest pressure drop where an increase is expected.

**Nyckelord**  
Keyword

Throttle, Discharge Coefficient, Heat Transfer, CFD, Surface Roughness